Damped (linear) response theory within the resolution-of-identity coupled cluster singles and approximate doubles (RI-CC2) method

Fedotov, Daniil ; Coriani, Sonia; Hättig, Christof

Published in:
Journal of Chemical Physics

Link to article, DOI:
10.1063/5.0042759

Publication date:
2021

Document Version
Publisher's PDF, also known as Version of record

The Journal of Chemical Physics

Damped (linear) response theory within the resolution-of-identity coupled cluster singles and approximate doubles (RI-CC2) method

Cite as: J. Chem. Phys. **154**, 124110 (2021); https://doi.org/10.1063/5.0042759
Submitted: 03 January 2021 . Accepted: 04 March 2021 . Published Online: 23 March 2021

Daniil A. Fedotov, Sonia Coriani, and Christof Hättig

The Journal of Chemical Physics ARTICLE scitation.org/journal/jcp

Damped (linear) response theory within the resolution-of-identity coupled cluster singles and approximate doubles (RI-CC2) method

Cite as: J. Chem. Phys. 154, 124110 (2021); doi: 10.1063/5.0042759
Submitted: 3 January 2021 • Accepted: 4 March 2021 •
Published Online: 23 March 2021

Daniil A. Fedotov,[1] Sonia Coriani,[1,a)] and Christof Hättig[2,a)]

AFFILIATIONS

[1] DTU Chemistry, Technical University of Denmark, Kemitorvet Bldg. 207, DK-2800 Kongens Lyngby, Denmark
[2] Arbeitsgruppe Quantenchemie, Ruhr-Universität Bochum, D-44780 Bochum, Germany

[a)] **Authors to whom correspondence should be addressed:** soco@kemi.dtu.dk and christof.haettig@rub.de

ABSTRACT

An implementation of a complex solver for the solution of the linear equations required to compute the complex response functions of damped response theory is presented for the resolution-of-identity (RI) coupled cluster singles and approximate doubles (CC2) method. The implementation uses a partitioned formulation that avoids the storage of double excitation amplitudes to make it applicable to large molecules. The solver is the keystone element for the development of the damped coupled cluster response formalism for linear and nonlinear effects in resonant frequency regions at the RI-CC2 level of theory. Illustrative results are reported for the one-photon absorption cross section of C_{60}, the electronic circular dichroism of n-helicenes (n = 5, 6, 7), and the C_6 dispersion coefficients of a set of selected organic molecules and fullerenes.

I. INTRODUCTION

Damped response theory[1] and the conceptually equivalent complex polarization propagator (CPP) approach[2–11] are increasingly popular frameworks to compute resonance convergent response functions and thereby simulate a variety of spectroscopic effects. They have proven particularly convenient in cases where traditional calculations of explicit excited states (i.e., of individual excitation energies as eigenvalues and corresponding oscillator strengths, also known as "stick" spectra) are impractical due to a large density of states—a prototypical example being the absorption spectrum of large molecules with many equivalent atoms in extended basis sets over a broad frequency range. They allow to specifically target a given spectral region, hereby bypassing the calculation of lower-lying states. They are also advantageous in that they give access to molecular properties in (additional) resonant conditions, as in two-photon absorption (TPA)[7,12] and resonant inelastic x-ray scattering (RIXS).[10,13] In addition, the CPP approach can be used to compute, e.g., polarizabilities at imaginary frequencies that are needed for the calculation of C_6 dispersion coefficients.[8,14,15]

Damped response/CPP frameworks have been successfully implemented at various levels of theory, from Hartree–Fock and time-dependent density functional theory[2–4,16] to multiconfigurational self-consistent field,[2,3] Algebraic Diagrammatic Construction (ADC),[15,17] and Coupled-Cluster (CC) theory.[8–10,18] Extensions to solvated environments (embedding and solvation models)[19,20] and the relativistic domain[21,22] have also been presented.

Applications to date include linear properties such as one-photon absorption (OPA) and electronic circular dichroism (ECD) in different frequency regions (from UV to x ray),[5,6,9,18,23,24] C_6 dispersion coefficients computed from polarizabilities at imaginary frequencies,[8,14,15] non-linear effects such as magnetic-field induced circular dichroism (MCD) and nuclear-spin induced circular

dichroism (NSCD),[25–27] magneto-chiral dichroism (MChD) and magneto-chiral birefringence (MChB) dispersion,[28] two-photon absorption in both UV–Vis and x-ray regimes,[7,12] and resonant inelastic x-ray scattering.[10,13,24,29]

A keystone element of all damped response/CPP frameworks is the solution of the (linear) response equations for a complex, or damped, frequency.[11] An implementation of a complex linear response solver within a coupled cluster framework was presented by Kauczor *et al.*[18] for the response of the cluster amplitudes and later extended to the response of the Lagrange multipliers by Faber and Coriani,[10] in both cases using an algorithm that assumes the storage of amplitudes or multipliers for all excitation classes (*vide infra*). Specific strategies to eliminate convergence issues in the x-ray frequency range have been discussed by Faber and Coriani[24] and by Nanda *et al.*[29] Here, we extend the complex solver of Ref. 18 to the case of the resolution-of-identity (RI) coupled cluster singles and approximate doubles (CC2) method as implemented in the Turbomole package,[30,31] which employs a partitioned formulation that avoids the storage of amplitudes and multipliers for double excitation. This is important for large scale applications of CC2, which would otherwise be hampered by I/O and storage demands. As illustrative results, we report the UV–Vis OPA spectra of C_{60}, the ECD spectra of three helicenes, and the ground-state C_6 dispersion coefficients of a set of organic molecules previously studied in the literature with other *ab initio* methods.

II. THEORY

A. The CC complex linear response function: Definitions and properties of interest

In CC damped linear response theory,[8–10,18] we compute the complex polarizability as

$$\langle\langle x;y\rangle\rangle_{\omega+i\gamma} = \frac{1}{2}\hat{C}^{\pm\omega}\{\eta^x t^y(\omega+i\gamma) + \eta^y t^x(-\omega-i\gamma) + \mathbf{F}t^y(\omega+i\gamma)t^x(-\omega-i\gamma)\}, \tag{1}$$

where $\hat{C}^{\pm\omega}$ is a symmetrization operator, defined as $\hat{C}^{\pm\omega}f(\omega) = f(\omega) + f^*(-\omega)$. Note that the symmetrization operator only turns the sign of the real frequency ω. In Eq. (1), $\mathbf{F}$ is the matrix of second derivatives (at zero field strength) of the CC Lagrangian $\mathcal{L}$ with respect to cluster amplitudes, $F_{\mu\nu} = \left(\frac{\partial^2\mathcal{L}}{\partial t_\mu \partial t_\nu}\right)$, and the vector η^y is the second derivative of the Lagrangian with respect to cluster amplitudes and the field strength ε_y, $\eta^y_\mu = \left(\frac{\partial^2\mathcal{L}}{\partial t_\mu \partial \varepsilon_y}\right)$. We refer to, e.g., Ref. 32 for the general definitions of vectors and matrices of response functions in CC response theory. The specific CC2 expressions can be found, e.g., in Ref. 33. The solution of the response equations yielding the amplitudes $t^y(\omega+i\gamma)$ within the RI-CC2 framework is discussed in Sec. II B. Here, we only note that $\mathbf{F}$ and (for real operators x and y) also η^y are purely real, while the amplitude responses fulfill the symmetry

$$t^x(\omega+i\gamma)^* = t^x(\omega-i\gamma). \tag{2}$$

If both operators are real and only diagonal components are considered, the real and imaginary parts of the complex dipole–dipole polarizability in Eq. (1) are

$$\Re\langle\langle x;x\rangle\rangle_{\omega+i\gamma} = \eta^x_\Re\, t^x_\Re(\omega+i\gamma) + \eta^x_\Re\, t^x_\Re(-\omega-i\gamma) + \mathbf{F}t^x_\Re(\omega+i\gamma)t^x_\Re(-\omega-i\gamma) - \mathbf{F}t^x_\Im(-\omega-i\gamma)t^x_\Im(\omega+i\gamma), \tag{3}$$

$$\Im\langle\langle x;x\rangle\rangle_{\omega+i\gamma} = \eta^x_\Re\, t^x_\Im(\omega+i\gamma) + \eta^x_\Re\, t^x_\Im(-\omega-i\gamma) + \mathbf{F}t^x_\Im(\omega+i\gamma)t^x_\Re(-\omega-i\gamma) + \mathbf{F}t^x_\Im(-\omega-i\gamma)t^x_\Re(\omega+i\gamma), \tag{4}$$

where we have explicitly split the complex response amplitudes into real and imaginary parts,

$$t^x(\omega+i\gamma) = t^x_\Re(\omega+i\gamma) + i\; t^x_\Im(\omega+i\gamma). \tag{5}$$

The imaginary part of polarizability can be used to compute, for instance, OPA cross sections,

$$\sigma_{\mathrm{OPA}}(\omega) \propto \omega\, \Im\langle\langle \mu_\alpha;\mu_\alpha\rangle\rangle_{\omega+i\gamma}, \tag{6}$$

where μ_α is the α-component of the electric dipole operator, and the incident frequency ω is chosen within the specific region of interest, e.g., UV–Vis or x ray. The polarizability dispersion profiles, illustrating the variation of the dipole polarizability over a given frequency range, can conversely be obtained from the real part of the complex dipole polarizability.

If one of the two operators in the linear response function, say, $\mathcal{X}$, is purely imaginary, we have

$$t^{\mathcal{X}}(\omega+i\gamma)^* = -t^{\mathcal{X}}(\omega-i\gamma), \tag{7}$$

and it is the real part of the complex response function that yields the absorption component,

$$\begin{aligned}\Re\langle\langle x;\mathcal{X}\rangle\rangle_{\omega+i\gamma} = \tfrac{1}{2}\Big\{&\eta^x_\Re\, t^{\mathcal{X}}_\Re(\omega+i\gamma) - \eta^x_\Re\, t^{\mathcal{X}}_\Re(-\omega-i\gamma) \\ &- \eta^{\mathcal{X}}_\Im\, t^x_\Im(-\omega-i\gamma) + \eta^{\mathcal{X}}_\Im\, t^x_\Im(\omega+i\gamma) \\ &+ \mathbf{F}t^x_\Re(-\omega-i\gamma)t^{\mathcal{X}}_\Re(\omega+i\gamma) + \mathbf{F}t^x_\Re(\omega+i\gamma) \\ &\times t^{\mathcal{X}}_\Re(-\omega-i\gamma) - \mathbf{F}t^x_\Im(-\omega-i\gamma)t^{\mathcal{X}}_\Im(\omega+i\gamma) \\ &- \mathbf{F}t^x_\Im(\omega+i\gamma)t^{\mathcal{X}}_\Im(-\omega-i\gamma)\Big\}.\end{aligned} \tag{8}$$

A prototypical case described by such a response function is the ECD cross section—most often expressed as the difference $\Delta\varepsilon$ in extinction coefficients for left and right circularly polarized light—in the length gauge (lg),

$$\Delta\varepsilon^{\mathrm{lg}}(\omega) \propto \omega\, \Re\langle\langle m_\alpha;\mu_\alpha\rangle\rangle_{\omega+i\gamma}, \tag{9}$$

whereas the optical rotation dispersion (ORD) profile is given by the imaginary part,

$$\sigma_{\mathrm{ORD}}^{\mathrm{lg}}(\omega) \propto \omega\, \Im\langle\langle m_\alpha; \mu_\alpha\rangle\rangle_{\omega+i\gamma}. \tag{10}$$

We note in passing that, in cases such as ORD and ECD, the symmetric form of the (complex) polarizability requires solving the complex response equations for both imaginary and real operators. Alternatively, one can resort to the asymmetric form

$$\langle\langle \mathcal{X}; x\rangle\rangle_{\omega+i\gamma} = \frac{1}{2}\hat{C}^{\pm\omega}\left\{\bar{t}^x(\omega+i\gamma)\xi^{\mathcal{X}} + \eta^{\mathcal{X}}t^x(\omega+i\gamma)\right\}, \tag{11}$$

which, thus, requires the solution of the CPP equations for the left response multipliers $\bar{t}^x(\omega+i\gamma)$,

$$\bar{t}^x(\omega+i\gamma)[\mathbf{A} + (\omega+i\gamma)\mathbf{1}] = -\eta^x - \mathbf{F}t^x(\omega+i\gamma), \tag{12}$$

along with those for the response amplitudes $t^x(\omega + i\gamma)$, for the real operator x. This allows one to bypass the solution of the response vectors for the imaginary operator. The first-order (complex) Lagrange multipliers are also needed for higher-order response and transition properties, such as the previously mentioned two-photon absorption, RIXS, and MCD.[10,34]

The length-gauge expressions of the optical rotation (OR) tensor and of the rotatory strengths within resonant response theory are gauge-origin dependent. Conversely, the velocity-gauge forms, which involve two imaginary operators, namely, the linear momentum p_α and the magnetic moment m_α, are origin independent.[35] Within CC theory, the "modified" velocity gauge expression of the OR tensor is typically used,[36,37]

$$G_{\alpha\alpha}^{\mathrm{mv}}(\omega) = \omega^{-1}\left\{\langle\langle p_\alpha; m_\alpha\rangle\rangle_\omega - \langle\langle p_\alpha; m_\alpha\rangle\rangle_0\right\}, \tag{13}$$

which ensures that the thus-computed OR tensor is zero in the limit of zero frequency, as it should be according to exact theory. We generalize the above expression to obtain the CPP optical rotatory dispersion and the electronic circular dichroism in the modified velocity gauge,

$$\sigma_{\mathrm{ORD}}^{\mathrm{mv}}(\omega) \propto \Re\left\{\langle\langle p_\alpha; m_\alpha\rangle\rangle_{\omega+i\gamma} - \langle\langle p_\alpha; m_\alpha\rangle\rangle_0\right\} \tag{14}$$

and

$$\Delta\varepsilon^{\mathrm{mv}}(\omega) \propto \Im\left\{\langle\langle p_\alpha; m_\alpha\rangle\rangle_{\omega+i\gamma} - \langle\langle p_\alpha; m_\alpha\rangle\rangle_0\right\} = \Im\langle\langle p_\alpha; m_\alpha\rangle\rangle_{\omega+i\gamma}. \tag{15}$$

Note that the correction to the ECD expression is redundant, since the imaginary part of the (real) response function is zero at the static limit. An alternative choice of CPP expression is to use a lifetime parameter that is scaled with the real frequency,

$$\langle\langle p_\alpha, m_\alpha\rangle\rangle_{\omega(1+i\gamma)} - \langle\langle p_\alpha, m_\alpha\rangle\rangle_0. \tag{16}$$

This is a slightly different approach than the one typically used with the CPP, again with no correction for ECD. It would have the formal advantage of conserving the symmetry $\sigma_{\mathrm{ORD}}(-\omega) = -\sigma_{\mathrm{ORD}}(\omega)$. This alternative expression would only be advantageous over the first one in practical applications where ω and γ are of similar magnitude, or when $\gamma > \omega$, for instance, because one scans with ω through 0. If one is interested in computing, for instance, $\sigma_{\mathrm{ECD}}(\omega)$ for the UV–Vis region with γ of the order of 0.1 eV, the first expression is to be preferred. This is the case here, so all ECD results presented in the following are obtained according to Eq. (14).

Finally, within damped linear response theory, one can also straightforwardly compute the isotropic dipole–dipole polarizability at purely imaginary frequencies, $\overline{\alpha}(i\omega)$, by setting the real frequency equal to zero and $\gamma = \omega$ in Eq. (1). From the isotropic averaged polarizability at imaginary frequency, one can then obtain coefficients to describe the long-range part of London dispersion interactions, e.g., the C_6 dispersion coefficients,[8,14,15]

$$C_6 = \frac{3\hbar}{\pi}\int_0^\infty \overline{\alpha}^A(i\omega)\overline{\alpha}^B(i\omega)d\omega, \tag{17}$$

where A and B label the interacting systems. The C_6 dispersion coefficients can be used, e.g., to compute the long-range dispersion interaction energy between A and B, also known as the Casimir–Polder potential, according to the simplified expression valid in the van der Waals region,[15] as $\Delta E(R_{AB}) = -\frac{\hbar}{\pi}\frac{C_6}{R_{AB}^6}$, and to determine long-range dispersion interaction corrections to density functional theory.[38–40]

B. The complex linear response equations for (RI-)CC2

The properties defined in Sec. II A entail the solution of complex response equations to obtain the real and imaginary components of the response amplitudes $t^x(\omega + i\gamma)$ and multipliers $\bar{t}^x(\omega + i\gamma)$,

$$\{\mathbf{A} - (\omega+i\gamma)\mathbf{1}\}t^x(\omega+i\gamma) = -\xi^x, \tag{18}$$

$$\bar{t}^x(\omega+i\gamma)\{\mathbf{A} + (\omega+i\gamma)\mathbf{1}\} = -\eta^x - \mathbf{F}t^x(\omega+i\gamma), \tag{19}$$

where $\mathbf{A}$ is the CC Jacobian, $A_{\mu\nu} = \left(\frac{\partial^2\mathcal{L}}{\partial\bar{t}_\mu\partial t_\nu}\right)$, and $\xi_\mu^x = \left(\frac{\partial^2\mathcal{L}}{\partial\bar{t}_\mu\partial\varepsilon_x}\right)$.[32] We refer once again to, e.g., Refs. 33, 41, and 42 for specific definitions of the CC2 right-hand-side (RHS) vectors ξ^x and η^x and of the matrices $\mathbf{A}$ and $\mathbf{F}$. We will in the following concentrate solely on the solution of Eq. (18) within RI-CC2 without storing any double excitation amplitudes, multipliers, or trial vectors. For this, we start from the complex linear response equations in the matrix form of Ref. 18 and explicitly partition them in singles (S) and doubles (D) blocks. For ease of notation, we omit in the following the frequency argument on the response amplitudes and write

$$\begin{bmatrix} \mathbf{A}_{SS} - \omega\mathbf{1}_{SS} & \mathbf{A}_{SD} & \gamma\mathbf{1}_{SS} & \mathbf{0} \\ \mathbf{A}_{DS} & \mathbf{A}_{DD} - \omega\mathbf{1}_{DD} & \mathbf{0} & \gamma\mathbf{1}_{DD} \\ -\gamma\mathbf{1}_{SS} & \mathbf{0} & \mathbf{A}_{SS} - \omega\mathbf{1}_{SS} & \mathbf{A}_{SD} \\ \mathbf{0} & -\gamma\mathbf{1}_{DD} & \mathbf{A}_{DS} & \mathbf{A}_{DD} - \omega\mathbf{1}_{DD} \end{bmatrix} \begin{bmatrix} t^x_{\Re,S} \\ t^x_{\Re,D} \\ t^x_{\Im,S} \\ t^x_{\Im,D} \end{bmatrix} = -\begin{bmatrix} \xi^x_{\Re,S} \\ \xi^x_{\Re,D} \\ \xi^x_{\Im,S} \\ \xi^x_{\Im,D} \end{bmatrix} \tag{20}$$

equivalent to the system of equations

$$\begin{cases} (\mathbf{A}_{SS} - \omega \mathbf{1}_{SS})\, t^x_{\Re,S} + \gamma\, t^x_{\Im,S} = -\xi^x_{\Re,S} - \mathbf{A}_{SD} t^x_{\Re,D}, & \text{(21a)} \\ (\mathbf{A}_{DD} - \omega \mathbf{1}_{DD}) t^x_{\Re,D} + \gamma\, t^x_{\Im,D} = -\xi^x_{\Re,D} - \mathbf{A}_{DS} t^x_{\Re,S}, & \text{(21b)} \\ (\mathbf{A}_{SS} - \omega \mathbf{1}_{SS})\, t^x_{\Im,S} - \gamma\, t^x_{\Re,S} = -\xi^x_{\Im,S} - \mathbf{A}_{SD} t^x_{\Im,D}, & \text{(21c)} \\ (\mathbf{A}_{DD} - \omega \mathbf{1}_{DD})\, t^x_{\Im,D} - \gamma\, t^x_{\Re,D} = -\xi^x_{\Im,D} - \mathbf{A}_{DS} t^x_{\Im,S}. & \text{(21d)} \end{cases}$$

Assuming we work with canonical molecular orbitals, the doubles–doubles block $\mathbf{A}_{DD}$ of the CC2 Jacobian is diagonal, and so is in this case the doubles–doubles resolvent matrix,[41] $\mathbf{R}_{DD} = -[\mathbf{A}_{DD} - (\omega + i\gamma)\mathbf{1}_{DD}]^{-1}$. We, therefore, define

$$\mathbf{\Delta} = (\mathbf{A}_{DD} - \omega \mathbf{1}_{DD}), \tag{22}$$

with the diagonal elements

$$\Delta^{ij}_{ab} = (\varepsilon_a - \varepsilon_i + \varepsilon_b - \varepsilon_j - \omega). \tag{23}$$

We isolate $t^x_{\Im,D}$ from Eq. (21d) and $t^x_{\Re,D}$ from Eq. (21b), and introduce each resulting expression into the other, to arrive at

$$t^x_{\Re,D} = -\frac{\Delta}{\gamma^2 + \Delta^2}\left(\xi^x_{\Re,D} + \mathbf{A}_{DS} t^x_{\Re,S}\right) + \frac{\gamma}{\gamma^2 + \Delta^2}\left(\xi^x_{\Im,D} + \mathbf{A}_{DS} t^x_{\Im,S}\right), \tag{24}$$

$$t^x_{\Im,D} = -\frac{\Delta}{\gamma^2 + \Delta^2}\left(\xi^x_{\Im,D} + \mathbf{A}_{DS} t^x_{\Im,S}\right) - \frac{\gamma}{\gamma^2 + \Delta^2}\left(\xi^x_{\Re,D} + \mathbf{A}_{DS} t^x_{\Re,S}\right). \tag{25}$$

Inserting Eq. (24) into Eq. (21c) and Eq. (25) into Eq. (21c), we finally obtain the effective CC2 CPP linear response equations in the compact matrix form,

$$\begin{bmatrix} \mathbf{A}^{\text{eff}}_{SS}(\omega,\gamma) - \omega \mathbf{1}_{SS} & -\mathbf{\Gamma}^{\text{eff}}_{SS}(\omega,\gamma) + \gamma \mathbf{1}_{SS} \\ \mathbf{\Gamma}^{\text{eff}}_{SS}(\omega,\gamma) - \gamma \mathbf{1}_{SS} & \mathbf{A}^{\text{eff}}_{SS}(\omega,\gamma) - \omega \mathbf{1}_{SS} \end{bmatrix} \begin{bmatrix} t^x_{\Re,S} \\ t^x_{\Im,S} \end{bmatrix} = -\begin{bmatrix} \xi^{x,\text{eff}}_{\Re,S}(\omega,\gamma) \\ \xi^{x,\text{eff}}_{\Im,S}(\omega,\gamma) \end{bmatrix}, \tag{26}$$

where

$$\mathbf{A}^{\text{eff}}_{SS}(\omega,\gamma) = \mathbf{A}_{SS} - \mathbf{A}_{SD}\frac{\Delta}{\Delta^2 + \gamma^2}\mathbf{A}_{DS}, \tag{27}$$

$$\mathbf{\Gamma}^{\text{eff}}_{SS}(\omega,\gamma) = -\mathbf{A}_{SD}\frac{\gamma}{\Delta^2 + \gamma^2}\mathbf{A}_{DS} \tag{28}$$

and

$$\xi^{x,\text{eff}}_{\Re,S}(\omega,\gamma) = \xi^x_{\Re,S} - \mathbf{A}_{SD}\frac{\Delta}{\Delta^2 + \gamma^2}\xi^x_{\Re,D} + \mathbf{A}_{SD}\frac{\gamma}{\Delta^2 + \gamma^2}\xi^x_{\Im,D}, \tag{29}$$

$$\xi^{x,\text{eff}}_{\Im,S}(\omega,\gamma) = \xi^x_{\Im,S} - \mathbf{A}_{SD}\frac{\Delta}{\Delta^2 + \gamma^2}\xi^x_{\Im,D} - \mathbf{A}_{SD}\frac{\gamma}{\Delta^2 + \gamma^2}\xi^x_{\Re,D}. \tag{30}$$

Thus, the CPP(-RI)-CC2 building blocks are the same as in the standard linear response case,[42,43] just with slightly different generalized values for the diagonal elements of the resolvent as scaling factors. These scaling factors are exactly the same as used in the preconditioning step in Ref. 18.

III. IMPLEMENTATION

A. The iterative CPP solver

The general strategy for the implementation of our solver consists in working exclusively with real trial vectors, generating two new vectors at each iteration from the real and imaginary parts of the preconditioned residual vectors, and solving the complex linear response equation (27) in the reduced space. In detail, the fundamental steps of the iterative solver are the following:

1. *Generation of the start trial vectors* by preconditioning the effective RHS vectors:

$$(\tilde{b}_1)_{ai} = \frac{\varepsilon_a - \varepsilon_i - \omega}{(\varepsilon_a - \varepsilon_i - \omega)^2 + \gamma^2}\xi^{x,\text{eff}}_{\Re,ai} + \frac{\gamma}{(\varepsilon_a - \varepsilon_i - \omega)^2 + \gamma^2}\xi^{x,\text{eff}}_{\Im,ai} \tag{31}$$

and

$$(\tilde{b}_2)_{ai} = \frac{\varepsilon_a - \varepsilon_i - \omega}{(\varepsilon_a - \varepsilon_i - \omega)^2 + \gamma^2}\xi^{x,\text{eff}}_{\Im,ai} - \frac{\gamma}{(\varepsilon_a - \varepsilon_i - \omega)^2 + \gamma^2}\xi^{x,\text{eff}}_{\Re,ai}, \tag{32}$$

followed by orthonormalization.

2. *Computation of the linearly transformed vectors:*

$$\sigma^{\Re}_1 = \mathbf{A}^{\text{eff}} b_1, \quad \sigma^{\Re}_2 = \mathbf{A}^{\text{eff}} \boldsymbol{b}_2, \quad \sigma^{\Im}_1 = \mathbf{\Gamma}^{\text{eff}} b_1, \quad \sigma^{\Im}_2 = \mathbf{\Gamma}^{\text{eff}} b_2. \tag{33}$$

3. *Computation of the reduced-space building blocks:*

$$\mathbf{A}^{\text{red}}_{ij} = b^T_i \sigma^{\Re}_j, \qquad \mathbf{\Gamma}^{\text{red}}_{ij} = b^T_i \sigma^{\Im}_j, \tag{34}$$

$$\xi^{x,\text{red}}_{\Re,i} = b^T_i \xi^{x,\text{eff}}_{\Re}, \quad \xi^{x,\text{red}}_{\Im,i} = b^T_i \xi^{x,\text{eff}}_{\Im}, \tag{35}$$

where i and j run on the number of trial vectors. Note that $n_{\text{red}} = 2n$, where n is the iteration number.

4. *Construction and solution of the CPP equation in the reduced space:*

$$\begin{bmatrix} \mathbf{A}^{\text{red}} - \omega \mathbf{1} & -\mathbf{\Gamma}^{\text{red}} + \gamma \mathbf{1} \\ \mathbf{\Gamma}^{\text{red}} - \gamma \mathbf{1} & \mathbf{A}^{\text{red}} - \omega \mathbf{1} \end{bmatrix} \begin{bmatrix} x^{\Re} \\ x^{\Im} \end{bmatrix} = -\begin{bmatrix} \xi^{x,\text{red}}_{\Re}(\omega) \\ \xi^{x,\text{red}}_{\Im}(\omega) \end{bmatrix}. \tag{36}$$

The CPP reduced equation is solved using standard library solvers to obtain $x^{\Re}$ and $x^{\Im}$.

5. *Construction of the solution and residual vectors in the full (singles) space*: The solution vectors at iteration n are linear combinations of the trial basis with the reduced space solution vectors as coefficients,

$$t^{x,(n)}_{\Re} = \sum_i^{n_{\text{red}}} x^{\Re}_i \boldsymbol{b}_i, \quad t^{x,(n)}_{\Im} = \sum_i^{n_{\text{red}}} x^{\Im}_i \boldsymbol{b}_i. \tag{37}$$

They are formally introduced in the effective CPP equation to yield the residual vectors

$$R^{(n)}_{\Re,S} = \sum_i^{n_{\text{red}}} x_i^{\Re}\sigma_{i,S}^{\Re} - \omega\, t^{x,(n)}_{\Re,S} - \sum_i^{n_{\text{red}}} x_i^{\Im}\sigma_{i,S}^{\Im} + \gamma\, t^{x,(n)}_{\Im,S} + \xi^{x,\text{eff}}_{\Re,S}, \quad (38)$$

$$R^{(n)}_{\Im,S} = \sum_i^{n_{\text{red}}} x_i^{\Im}\sigma_{i,S}^{\Re} - \omega t^{x,(n)}_{\Im,S} + \sum_i^{n_{\text{red}}} x_i^{\Re}\sigma_{i,S}^{\Im} - \gamma\, t^{x,(n)}_{\Re,S} + \xi^{x,\text{eff}}_{\Im,S}. \quad (39)$$

Solution and residual vectors are, alike the linearly transformed one, stored as vectors that are twice the size of a singles amplitude.

6. *Generation of the new trial vectors from the preconditioned residuals:* If the residual vectors of step 5 are larger than a preset threshold, new trial vectors are generated and a new iteration is made. In practice, we split the (tentative) trial vector into two vectors,

$$(\tilde{b}_{2n-1})_{ai} = \frac{\varepsilon_a - \varepsilon_i - \omega}{(\varepsilon_a - \varepsilon_i - \omega)^2 + \gamma^2}\cdot R^{(n)}_{\Re,ai} + \frac{\gamma}{(\varepsilon_a - \varepsilon_i - \omega)^2 + \gamma^2}\cdot R^{(n)}_{\Im,ai}, \quad (40)$$

$$(\tilde{b}_{2n})_{ai} = \frac{\varepsilon_a - \varepsilon_i - \omega}{(\varepsilon_a - \varepsilon_i - \omega)^2 + \gamma^2}\cdot R^{(n)}_{\Im,ai} - \frac{\gamma}{(\varepsilon_a - \varepsilon_i - \omega)^2 + \gamma^2}\cdot R^{(n)}_{\Re,ai}, \quad (41)$$

which are normalized and then orthogonalized onto the previous trial vectors. If, after this step, their norm is smaller than a linear-dependence threshold, they are discarded; otherwise, they are normalized once more and added to the set of trial vectors.

7. *Extension of the reduced space and iteration until convergence:* If the residuals for all equations have decreased below a user-defined threshold, the procedure is stopped, or else the reduced space is extended as in step 3 and steps 4–6 are repeated until convergence.

B. Building blocks: The RHS vectors

The perturbation operators are in general assumed to be either real or purely imaginary. As a consequence, the (not partitioned) RHS vectors ξ^x for the first-order amplitude equations are either real or purely imaginary. In the case of real perturbations (e.g., electric dipole), the effective RHS vectors simplify to

$$\xi^{x,\text{eff}}_{\Re,S}(\omega,\gamma) = \xi^x_S - \mathbf{A}_{SD}\frac{\Delta}{\Delta^2+\gamma^2}\xi^x_D, \quad (42)$$

$$\xi^{x,\text{eff}}_{\Im,S}(\omega,\gamma) = -\mathbf{A}_{SD}\frac{\gamma}{\Delta^2+\gamma^2}\xi^x_D. \quad (43)$$

Within RI-CC2, the doubles elements of the RHS vector ξ^x_D are computed only on the fly and immediately contracted with the elements of the singles–doubles block of the Jacobian matrix $\mathbf{A}_{SD}$, in a loop either over pairs of occupied or over pairs of virtual orbital indices. This entails computing

$$(\tilde{\xi}^x_{\Re})^{ij}_{ab} = \frac{-\Delta_{aibj}}{\Delta^2_{aibj}+\gamma^2}\xi^{x,ij}_{ab}, \quad (44)$$

$$(\tilde{\xi}^x_{\Im})^{ij}_{ab} = \frac{-\gamma}{\Delta^2_{aibj}+\gamma^2}\xi^{x,ij}_{ab}, \quad (45)$$

where the elements of the unmodified doubles part of the RHS vector are[33]

$$\xi^{x,ij}_{ab} = \hat{P}^{ij}_{ab}\left(\sum_c t^{ij}_{ac}\hat{h}^x_{cb} - \sum_k t^{ik}_{ab}\hat{h}^x_{kj}\right). \quad (46)$$

Here, t^{ij}_{ab} are the zero-order double amplitudes and $\hat{h}^x_{pq}$ are the integrals of the one-electron operator x, similarity transformed with the exponential function of the single excitation cluster operator (for their definition, see Appendix B). $\hat{P}^{ij}_{ab}$ is a symmetrization operator, defined by $\hat{P}^{pr}_{qs}f_{pq,rs} = f_{pq,rs} + f_{rs,pq}$.[33]

Then, we contract $\tilde{\xi}^{x,ij}_{\Re,ab}$ and $\tilde{\xi}^{x,ij}_{\Im,ab}$ with the elements of the singles–doubles matrix $\mathbf{A}_{SD}$. In general, the contraction of $\mathbf{A}_{SD}$ with a doubles vector b^{kl}_{cd} can be written as[33]

$$\sum_{ckdl} A_{ai,ckdl}b^{kl}_{cd} = +\sum_{cdk}\left(2b^{ik}_{cd} - b^{ik}_{dc}\right)(kd\hat{|}ac) - \sum_{dkl}\left(2b^{kl}_{ad} - b^{kl}_{da}\right)(ld\hat{|}ki) + \sum_{ck}\left(2b^{ik}_{ac} - b^{ik}_{ca}\right)\hat{F}_{kc}, \quad (47)$$

where $\hat{F}_{kc}$ is the Fock matrix[43] and $(ld\hat{|}ki)$ are the two-electron integrals of the T_1-similarity transformed Hamiltonian operator (see their definition in Appendix B). Within RI-CC2, the two-electron integrals are approximated as[44–47]

$$(pq\hat{|}rs) = \sum_Q \hat{B}_{Q,pq}\hat{B}_{Q,rs}, \quad (48)$$

where

$$\hat{B}_{Q,pq} = \sum_P (pq\hat{|}P)V^{-\frac{1}{2}}_{PQ} = \sum_{\mu\nu}\Lambda^p_{\mu p}\Lambda^h_{\nu q}\sum_P(\mu\nu|P)V^{-\frac{1}{2}}_{PQ}. \quad (49)$$

In the last equality, $(\mu\nu|P)$ are three-index electron-repulsion integrals (ERIs) for the atomic orbitals μ, ν and the auxiliary basis function P and $V_{PQ} = (V|P)$ is a matrix containing as elements the two-index ERIs in the auxiliary basis. The Λ^p and Λ^h matrices are the T_1-transformed molecular orbital coefficients, whose definition is given in Appendix B. With this, the first two terms can be rewritten, e.g., as

$$\sum_{cdk}\left(2b^{ik}_{cd} - b^{ik}_{dc}\right)(kd\hat{|}ac) = \sum_{Qc}\left(\sum_{dk}\left(2b^{ik}_{cd} - b^{ik}_{dc}\right)\hat{B}_{Q,kd}\right)\hat{B}_{Q,ac} = \sum_{Qc}\bar{Y}_{Q,ci}\hat{B}_{Q,ac}, \quad (50)$$

where we introduced the $\bar{Y}$ intermediate

$$\bar{Y}_{Q,ai} = \sum_{bj}\left(2b^{ij}_{ab} - b^{ij}_{ba}\right)\hat{B}_{Q,jb}. \quad (51)$$

In the case of the CPP RHS vectors, these intermediates become

$$\bar{Y}^{x,\mathfrak{R}}_{Q,ai} = \sum_{bj}\left(2\tilde{\xi}^{x,ij}_{\mathfrak{R},ab} - \tilde{\xi}^{x,ij}_{\mathfrak{R},ba}\right)\hat{B}_{Q,jb}, \tag{52}$$

$$\bar{Y}^{x,\mathfrak{I}}_{Q,ai} = \sum_{bj}\left(2\tilde{\xi}^{x,ij}_{\mathfrak{I},ab} - \tilde{\xi}^{x,ij}_{\mathfrak{I},ba}\right)\hat{B}_{Q,jb}, \tag{53}$$

and the real and imaginary parts of the effective singles RHS vectors are computed as

$$\xi^{x,\mathrm{eff}}_{\mathfrak{R},ai} = \xi_{ai} + \sum_{ck}\left(2\tilde{\xi}^{x,ik}_{\mathfrak{R},ac} - \tilde{\xi}^{x,ik}_{\mathfrak{R},ca}\right)\hat{F}_{kc} + \sum_{cQ}\bar{Y}^{x,\mathfrak{R}}_{Q,ci}\hat{B}_{Q,ac} - \sum_{kQ}\bar{Y}^{x,\mathfrak{R}}_{Q,ak}\hat{B}_{Q,ki}, \tag{54}$$

$$\xi^{x,\mathrm{eff}}_{\mathfrak{I},ai} = \sum_{ck}\left(2\tilde{\xi}^{x,ik}_{\mathfrak{I},ac} - \tilde{\xi}^{x,ik}_{\mathfrak{I},ca}\right)\hat{F}_{kc} + \sum_{cQ}\bar{Y}^{x,\mathfrak{I}}_{Q,ci}\hat{B}_{Q,ac} - \sum_{kQ}\bar{Y}^{x,\mathfrak{I}}_{Q,ak}\hat{B}_{Q,ki}. \tag{55}$$

In case of an imaginary perturbation $\mathcal{X}$ (e.g., the magnetic dipole moment or the linear momentum), the effective RHS vector reads

$$\xi^{\mathcal{X},\mathrm{eff}}_{\mathfrak{R},S}(\omega,\gamma) = \mathbf{A}_{SD}\frac{+\gamma}{\Delta^2+\gamma^2}\xi^{\mathcal{X}}_{D}, \tag{56}$$

$$\xi^{\mathcal{X},\mathrm{eff}}_{\mathfrak{I},S}(\omega,\gamma) = \xi^{\mathcal{X}}_{S} + \mathbf{A}_{SD}\frac{-\Delta}{\Delta^2+\gamma^2}\xi^{\mathcal{X}}_{D}, \tag{57}$$

that is,

$$\xi^{\mathcal{X},\mathrm{eff}}_{\mathfrak{R},ai} = -\sum_{ck}\left(\tilde{\xi}^{\mathcal{X},ik}_{\mathfrak{R},ac} - \tilde{\xi}^{\mathcal{X},ik}_{\mathfrak{R},ca}\right)\hat{F}_{kc} - \sum_{cQ}\bar{Y}^{\mathcal{X},\mathfrak{R}}_{Q,ci}\hat{B}_{Q,ac} + \sum_{kQ}\bar{Y}^{\mathcal{X},\mathfrak{R}}_{Q,ak}\hat{B}_{Q,ki}, \tag{58}$$

$$\xi^{\mathcal{X},\mathrm{eff}}_{\mathfrak{I},ai} = \xi^{\chi}_{ai} + \sum_{ck}\left(2\tilde{\xi}^{\mathcal{X},ik}_{\mathfrak{I},ac} - \tilde{\xi}^{\mathcal{X},ik}_{\mathfrak{I},ca}\right)\hat{F}_{kc} + \sum_{cQ}\bar{Y}^{\mathcal{X},\mathfrak{I}}_{Q,ci}\hat{B}_{Q,ac} - \sum_{kQ}\bar{Y}^{\mathcal{X},\mathfrak{I}}_{Q,ak}\hat{B}_{Q,ki}. \tag{59}$$

C. Building blocks: The Jacobian transformation

To build the reduced-space quantities needed in the CPP solver, we need, for each trial vector b, the result of its transformations with the effective matrices $\mathbf{A}^{\mathrm{eff}}_{SS}(\omega,\gamma)$ and $\mathbf{\Gamma}^{\mathrm{eff}}_{SS}(\omega,\gamma)$, typically referred to as σ vectors. To keep the overhead for the CPP small, the transformations with the two matrices are done together.

We express the result of the transformation of a singles trial vector b with the doubles–singles Jacobian matrix $\mathbf{A}_{DS}$ as one-index transformed two-electron integrals,

$$\sum_{ck}A_{aibj,ck}b_{ck} = \langle^{ij}_{ab}|[\hat{H},\tau_{ck}]\mathrm{HF}\rangle b_{ck} = (ai|\bar{bj}), \tag{60}$$

$$(ai|\bar{bj}) = \hat{P}^{ab}_{ij}\sum_{\alpha\beta\gamma\delta}\left(\bar{\Lambda}^{p}_{\alpha a}\Lambda^{h}_{\beta i} + \Lambda^{p}_{\alpha a}\bar{\Lambda}^{h}_{\beta i}\right)\Lambda^{p}_{\gamma b}\Lambda^{h}_{\delta j}(\alpha\beta|\gamma\delta), \tag{61}$$

where $\bar{\Lambda}^{p}$ and $\bar{\Lambda}^{h}$ are defined as in Appendix B, with the singles trial vector b_1 in place of the singles response amplitudes t^{x}_{1}. These four-index integrals are evaluated on the fly from three-center intermediates[43] [$\hat{B}_{Q,ai}$, Eq. (49), and $\tilde{B}_{Q,ai}$, given in Appendix B] and combined with the energy denominators from $\mathbf{\Delta}$ into intermediate doubles amplitudes. In other words, for the CPP implementation, the following intermediate doubles amplitudes are built:

$$\tilde{b}^{\mathfrak{R},ij}_{ab} = \frac{-\Delta_{aibj}}{\Delta^2_{aibj}+\gamma^2}(ai|\bar{bj}), \tag{62}$$

$$\tilde{b}^{\mathfrak{I},ij}_{ab} = \frac{-\gamma}{\Delta^2_{aibj}+\gamma^2}(ai|\bar{bj}). \tag{63}$$

With these, the transformations with $\mathbf{A}^{\mathrm{eff}}_{SS}$ and $\mathbf{\Gamma}^{\mathrm{eff}}_{SS}$ can be expressed as

$$\mathbf{A}^{\mathrm{eff}}_{SS}(\omega,\gamma)b_S = \mathbf{A}_{SS}b_S + \sum_{ckdl}\mathbf{A}_{S,ckdl}\tilde{b}^{\mathfrak{R},kl}_{cd}, \tag{64}$$

$$\mathbf{\Gamma}^{\mathrm{eff}}_{SS}(\omega,\gamma)b_S = \sum_{ckdl}\mathbf{A}_{S,ckdl}\tilde{b}^{\mathfrak{I},kl}_{cd}. \tag{65}$$

The contribution $\mathbf{A}_{SS}b_S$ is unchanged compared to the standard (non-CPP) solver.[41] The other contributions are evaluated in a way similar (and partially using the same routines) to the contributions to the effective right-hand sides discussed in Sec. III B,

$$\begin{aligned}\sigma^{\mathrm{eff}}_{\mathfrak{R},ai} &= \sum_{ck}A^{\mathrm{eff}}_{ai,ck}(\omega,\gamma)b_{ck}\\ &= \sum_{ck}A_{ai,ck}b_{ck} + \sum_{ck}\left(2\tilde{b}^{\mathfrak{R},ik}_{ac} - \tilde{b}^{\mathfrak{R},ik}_{ca}\right)\hat{F}_{kc}\\ &\quad + \sum_{cQ}\bar{Y}^{\mathfrak{R}}_{Q,ci}\hat{B}_{Q,ac} - \sum_{kQ}\bar{Y}^{\mathfrak{R}}_{Q,ak}\hat{B}_{Q,ki} + \sum_{ck}(2t^{ik}_{ac} - t^{ik}_{ca})\bar{F}_{kc}\end{aligned} \tag{66}$$

and

$$\begin{aligned}\sigma^{\mathrm{eff}}_{\mathfrak{I},ai} &= \sum_{ck}\Gamma^{\mathrm{eff}}_{ai,ck}(\omega,\gamma)b_{ck}\\ &= \sum_{ck}\left(2\tilde{b}^{\mathfrak{I},ik}_{ac} - \tilde{b}^{\mathfrak{I},ik}_{ca}\right)\hat{F}_{kc} + \sum_{cQ}\bar{Y}^{\mathfrak{I}}_{Q,ci}\hat{B}_{Q,ac} - \sum_{kQ}\bar{Y}^{\mathfrak{I}}_{Q,ak}\hat{B}_{Q,ki}.\end{aligned} \tag{67}$$

The real and imaginary $\bar{Y}$ intermediates are, as in Eq. (51), using the real and imaginary intermediate doubles amplitude trial vectors defined above.

D. The first-order perturbed densities

Once the real and imaginary response amplitudes have been obtained, we can build the real and imaginary linear response functions needed for the properties and spectra discussed in Sec. II A. This entails computing contractions of the (complex) response amplitudes with the η^{x} vectors and with the $\mathbf{F}$ matrix.

The contributions from the terms of the type $\eta^{x}\cdot t^{y}$ are formulated as contractions of densities and one-electron integrals of the perturbation operator,[33,43]

$$\eta^{x}\cdot t^{y} = \sum_{pq}D^{\eta}_{pq}(t^{y})\hat{h}^{x}_{pq}. \tag{68}$$

We do so as, for large systems, we do not want to store the doubles parts of η^x and t^y. In addition, to recalculate the doubles parts of both vectors for every dot product, i.e., for every pair of perturbations x and y, would require a number of $\mathcal{N}^5$-scaling steps that increase with the number of operator pairs. Via densities, on the other hand, the number of $\mathcal{N}^5$-scaling steps increases only linearly with the number of operators. The explicit density blocks are[43]

$$D^{\eta}_{ij}(t^x) = -\sum_a \bar{t}_{ja} t^x_{ai} - X^x_{ij}, \tag{69}$$

$$D^{\eta}_{ia}(t^x) = C^x_{ai} - \sum_k t^x_{ak} X_{ik} - \sum_b Y_{ba} t^x_{bi}, \tag{70}$$

$$D^{\eta}_{ai}(t^x) = 0, \tag{71}$$

$$D^{\eta}_{ab}(t^x) = \sum_i \bar{t}_{ia} t^x_{bi} + Y^x_{ba}. \tag{72}$$

The real part of $\mathbf{D}^{\eta}(t^x)$ is computed from the real part of t^x as in the standard response case.[43] The imaginary part of $\mathbf{D}^{\eta}(t^x)$ is done in the same way using the imaginary part of t^x. The contributions to the densities from the singles amplitudes are straightforward to compute since the singles are stored on disk and can be read from the file when needed. Complications arise from the doubles response amplitudes $t^{x,ij}_{ab}$, as they should also be implemented with $\mathcal{O}(\mathcal{N}^2)$-scaling memory demands. The expression of the doubles part of the response amplitudes is

$$t^{x,ij}_{ab} = -\left\{ \hat{P}^{ij}_{ab} \left(\sum_c t^{ij}_{ac} \hat{h}^x_{cb} - \sum_k t^{ik}_{ab} \hat{h}^x_{kj} \right) + (ai|bj)^x \right\} \Big/ (\varepsilon_a - \varepsilon_i + \varepsilon_b - \varepsilon_j - \omega - i\gamma). \tag{73}$$

The (complex) t^x_S-dressed four-index integrals are evaluated within the RI approximation as

$$(ai|bj)^x = \hat{P}^{ij}_{ab} \left\{ \sum_Q \bar{B}^{x,\Re}_{Q,ai} \hat{B}_{Q,bj} + i \sum_Q \bar{B}^{x,\Im}_{Q,ai} \hat{B}_{Q,bj} \right\}, \tag{74}$$

where the three-center intermediates $\bar{B}^{x,\Re}$ and $\bar{B}^{x,\Im}$ are built with, respectively, the real and imaginary parts of the singles amplitudes t^x_{ai}, see Appendix B.

As described elsewhere,[33,48] the ground-state double amplitudes are evaluated on the fly within the RI approximation and with a numerical Laplace transformation of the denominators,

$$t^{ij}_{ab} = \frac{-\sum_Q \hat{B}_{Q,ai} \hat{B}_{Q,bj}}{(\varepsilon_a - \varepsilon_i + \varepsilon_b - \varepsilon_j)} \approx -\sum_m \sum_Q \hat{K}^m_{Q,ai} \hat{K}^m_{Q,bj}, \tag{75}$$

with $\hat{K}^m_{Q,ai} = \hat{B}_{Q,ai} \sqrt{\omega_m} \exp\{-(\varepsilon_a - \varepsilon_i)\theta_m\}$, where θ_m are the Laplace sampling points and ω_m are the weights.[33] This allows us to do the transformation with the one-electron integrals for the perturbation operator x at the level of the $\hat{K}$ intermediates,[33]

$$\bar{K}^{m,x}_{Q,ai} = \sum_c \hat{K}^m_{Q,ci} \hat{h}^x_{ac} - \sum_k \hat{K}^m_{Q,ak} \hat{h}^x_{ki} \tag{76}$$

(assuming that x is purely real), so that we can compute the real and the imaginary response double amplitudes on the fly as

$$t^{x,ij}_{\Re,ab} = \hat{P}^{ij}_{ab} \left\{ -\sum_m \sum_Q \bar{K}^{m,x}_{Q,ai} \hat{K}^m_{Q,bj} + \sum_Q \bar{B}^{x,\Re}_{Q,ai} \hat{B}_{Q,bj} \right\} \times \frac{-\Delta_{aibj}}{\Delta^2_{aibj} + \gamma^2} - \hat{P}^{ij}_{ab} \sum_Q \bar{B}^{x,\Im}_{Q,ai} \hat{B}_{Q,bj} \cdot \frac{-\gamma}{\Delta^2_{aibj} + \gamma^2}, \tag{77}$$

$$t^{x,ij}_{\Im,ab} = \hat{P}^{ij}_{ab} \left\{ -\sum_m \sum_Q \bar{K}^{m,x}_{Q,ai} \hat{K}^m_{Q,bj} + \sum_Q \bar{B}^{x,\Re}_{Q,ai} \hat{B}_{Q,bj} \right\} \times \frac{-\gamma}{\Delta^2_{aibj} + \gamma^2} + \hat{P}^{ij}_{ab} \sum_Q \bar{B}^{x,\Im}_{Q,ai} \hat{B}_{Q,bj} \cdot \frac{-\Delta_{aibj}}{\Delta^2_{aibj} + \gamma^2}. \tag{78}$$

The doubles of the first-order response amplitudes are constructed in a loop over pairs of occupied orbitals i and j. In the same loop, the doubles of the ground-state Lagrange multipliers $\bar{t}^{ij}_{ab}$ are built. The response amplitudes $t^{x,ij}_{bc}$ are then contracted with the Lagrange multipliers to the intermediates

$$Y^x_{ab} = \sum_{cij} \bar{t}^{ij}_{ac} t^{x,ij}_{bc} \tag{79}$$

and

$$C^x_{ai} = \sum_{bj} \left(2t^{x,ij}_{ab} - t^{x,ij}_{ba} \right) \bar{t}_{jb}. \tag{80}$$

Then, the same procedure is repeated within a loop over pairs of virtual orbital indices a and b (with occupied and virtual orbitals interchanged) to calculate

$$X^x_{ik} = \sum_{abk} \bar{t}^{jk}_{ab} t^{x,ik}_{ab}. \tag{81}$$

The real and imaginary parts for the doubles are computed together to avoid having to compute the doubles multipliers twice, and thus, the real and imaginary parts of C^x, Y^x, and X^x are evaluated together. Eventually, the individual blocks of the density $\mathbf{D}^{\eta}(t^x)$ are put together from these intermediates and the singles parts for the response amplitudes and Lagrange multipliers.

E. The F-matrix contractions

Similar to the evaluation of $\eta^x \cdot t^y$, also the F-matrix contractions are organized such that all $\mathcal{O}(\mathcal{N}^5)$-scaling steps only depend on one perturbation, and only cheap, low-scaling, steps depend on both amplitude response vectors. The F-matrix contraction is first rewritten as

$$Ft^x t^y = \sigma^x \cdot t^y, \tag{82}$$

with

$$\sigma^x_\mu = \sum_{\nu=\nu_1,\nu_2} F_{\nu\mu} t^x_\nu. \tag{83}$$

The singles and doubles blocks of σ^x are partitioned as summarized in Table I. Algorithm 1 in Appendix B summarizes the main steps in the actual evaluation of the F-matrix contribution to the linear response function. Different from standard response theory, in the CPP case, all intermediates depending on the response amplitudes, i.e., carrying an upper index x or y, are complex. The contributions to the real and imaginary parts of the intermediates are evaluated with the real and imaginary parts of t^x, respectively, as described for standard response theory in Ref. 33.

The explicit evaluation of the doubles blocks is avoided by reformulating the contraction of σ^x_{iajb} with $t^{y,ij}_{ab}$ as in the following:

$$\frac{1}{2}\sum_{ijab}\sigma^{I,x}_{iajb}t^{y,ij}_{ab} = \frac{1}{2}\sum_{iajb}\hat{P}^{ij}_{ab}\left[\bar{t}_{ia}\left(2t^{y,ij}_{ab} - t^{y,ij}_{ba}\right)\right]\bar{F}^x_{jb} = \sum_{ia} C^y_{ai}\bar{F}^x_{ia}, \tag{84}$$

$$\frac{1}{2}\hat{P}^{ij}_{ab}\left(\sigma^{G,x}_{iajb} + \sigma^{H,x}_{iajb}\right)t^{y,ij}_{ab} = \sum_{jbQ}\left[-\sum_{ck}\left(\bar{t}_{jc}t^x_{ck}B_{Q,kb} + t^x_{ck}\bar{t}_{kb}B_{Q,jc}\right)\right]Y^y_{Q,bj} = \sum_{jbQ}\check{B}^x_{Q,jb}Y^y_{Q,bj}. \tag{85}$$

For the definition of the intermediates, we refer to Appendix B.

IV. RESULTS AND DISCUSSION

A. Computational details and cost estimates

The CPP solver for RI-CC2 has been implemented in a development version of the Turbomole program package.[31,49] The standard response calculations were performed using previously implemented RI-CC2 functionalities in Turbomole.[42,43] The excitation energies and strengths are given in the supplementary material.

The structure of C_{60} used in the OPA calculations was taken from Ref. 50. It originates from geometry optimization at the level of second-order Møller–Plesset Perturbation (MP2)[51] theory with

TABLE I. Singles and doubles blocks of σ^x. We refer to Appendix B for further definitions of intermediates.

$$\sigma^x_{ia} = \sigma^{0,x}_{ia} + \sigma^{F,x}_{ia} + \sigma^{JG,x}_{ia} + \sigma^{JH,x}_{ia} + \sigma^{I,x}_{ia} + \sigma^{J',x}_{ia}$$

$$\sigma^{0,x}_{ia} = 2\bar{F}^x_{ia}$$

$$\sigma^{F,x}_{ia} = \sum_{cdk}\bar{t}^{ki}_{cd}(ck|da)^x - \sum_{ckl}\bar{t}^{kl}_{ca}(ck|il)^x = \sum_{dQ}\left(\check{Y}^x_{Q,id}\hat{B}_{Q,da} + \check{Y}_{Q,id}\bar{B}^x_{Q,da}\right) - \sum_{lQ}\left(\check{Y}^x_{Q,al}\hat{B}_{Q,il} + \check{Y}_{Q,al}\bar{B}^x_{Q,il}\right)$$

$$\sigma^{JG,x}_{ia} = -\sum_j \bar{t}_{ja}\bar{F}^x_{ij} - \sum_j \bar{t}_{ja}\sum_{cdk}\left(2t^{x,jk}_{cd} - t^{x,kj}_{cd}\right)(kd|ic) = -\sum_j \bar{E}^{x,2}_{ij}\bar{t}_{ja}$$

$$\sigma^{JH,x}_{ia} = \sum_b \bar{t}_{ib}\bar{F}^x_{ba} + \sum_b \bar{t}_{ib}\sum_{dkl}\left(2t^{x,kl}_{bd} - t^{x,lk}_{bd}\right)(ld|ka) = \sum_b \bar{t}_{ib}\bar{E}^{x,1}_{ba}$$

$$\sigma^{I,x}_{ia} = \sum_{ck} C^x_{ck}[2(kc|ia) - (ic|ka)] = \sum_Q\left(2\sum_{ck}B_{Q,ck}C^x_{ck}\right)B_{Q,ia} - \sum_{Qk}\left(\sum_c B_{Q,ic}C^x_{ck}\right)B_{Q,ka}$$

$$= \sum_{Q\beta}\left\{2m^x_Q C_{\beta i} - \sum_k M^x_{Q,ik}C_{\beta k}\right\}B_{Q,\beta a}$$

$$\sigma^{J',x}_{ia} = \sum_{bj}\bar{t}_{jb}\left[2(bj|ia)^x - (ij|ba)^x\right]$$

$$= 2\sum_Q\left(\sum_{jb}\bar{B}^x_{Q,bj}\bar{t}_{jb}\right)B_{Q,ia} - \sum_{Qb}\left(\sum_j \bar{B}^x_{Q,ij}\bar{t}_{jb}\right)\sum_\beta \Lambda^p_{\beta b}\hat{B}_{Q,\beta a} - \sum_{Qb}\left(\sum_j \hat{B}_{Q,ij}\bar{t}_{jb}\right)\sum_\beta \bar{\Lambda}^{p,x}_{\beta b}\hat{B}_{Q,\beta a}$$

$$= 2\sum_Q \check{t}^x_Q B_{Q,ia} - \sum_{Qb}\left(\sum_j \bar{B}^x_{Q,ij}\bar{t}_{jb}\right)\sum_\beta \Lambda^p_{\beta b}\hat{B}_{Q,\beta a} - \sum_{Qb}\left(\sum_j \hat{B}_{Q,ij}\bar{t}_{jb}\right)\sum_\beta \bar{\Lambda}^{p,x}_{\beta b}\hat{B}_{Q,\beta a}$$

$$\sigma^x_{iajb} = \sigma^{I,x}_{iajb} + \sigma^{G,x}_{iajb} + \sigma^{H,x}_{iajb}$$

$$\sigma^{I,x}_{iajb} = 2\bar{t}_{ia}\bar{F}^x_{jb} - \bar{t}_{ja}\bar{F}^x_{ib}$$

$$\sigma^{G,x}_{iajb} = -\sum_{ck}\bar{t}_{jc}t^x_{ck}[2(kb|ia) - (ka|ib)]$$

$$\sigma^{H,x}_{iajb} = -\sum_{ck}t^x_{ck}\bar{t}_{ka}[2(jb|ic) - (jc|ib)]$$

Dunning's cc-pVTZ basis set.[52] The structures of the molecules considered for the C_6 coefficients (alkanes, unsaturated hydrocarbons, aldehydes, and ketones) are also MP2/cc-pVTZ optimized structures from the literature.[15] The Cartesian coordinates of all molecular systems considered are reported in the supplementary material. The structures of the helicenes[37] in the ECD calculations are MP2/cc-pVTZ optimized ones. According to the standard convention for helicoidal systems, we used (−)-5-helicene (M), (−)-6-helicene (M), and (+)-7-helicene (P) structures. The structures of the fullerenes in the C_6 calculations are the same B3LYP/cc-pVDZ optimized ones used in Ref. 53. In the calculations of the OPA spectra of C_{60}, we adopted the aug-cc-pVDZ basis set. The calculations of C_6 dispersion coefficients of the fullerenes were carried out using the cc-pVDZ basis set unless otherwise specified. For all other molecules, the aug-cc-pVTZ basis set was used. This also applies to the ECD calculations on the helicenes. The frozen-core approximation was used for the helicenes and in the calculations of the C_6 coefficients of the selected set of fullerenes. An optimized auxiliary basis set matching the chosen atomic orbital basis was employed in all calculations.[54]

For comparison with the CPP spectra, the individual oscillator strengths (and energies) were broadened using the Lorentzian function

$$g_j(\omega) = \frac{\gamma}{(\omega - \omega_j)^2 + \gamma^2}, \tag{86}$$

with half width at half maximum (HWHM) value $\gamma = 0.004\,556$ a.u. The frequency steps in the CPP calculations varied between 0.0025 and 0.01 a.u. A cubic spline was used for the interpolation between the computed points to obtain the CPP spectrum.

The C_6 coefficients were obtained according to Eq. (17), with $A = B$. The integral was evaluated using a Gauss–Legendre integration scheme, with a transformation of variables as suggested in Ref. 55 and followed by a Gauss–Legendre quadrature in the interval $-1 \le t \le +1$. A 12-point scheme was adopted.

To conclude this section, a brief comment is in place concerning the computational cost of a CPP calculation. The overall costs of response calculations depend, in addition to the system size and computed response properties, on several other factors, e.g., point group symmetry and the number of iterations for convergence. This makes a direct comparison between CPP and non-CPP calculations difficult as these calculations are in general quite different in nature and aim for different properties or, in the case of spectra, for different cases. However, the largest fraction of the computational time is usually spent for the solution of the response equations, which is dominated by the time needed for the linear transformations of trial vectors with the Jacobian matrix, $\sigma_i = \mathbf{A}b_i$. In the limit of a large system size $\mathcal{N}$, the operation count for these transformations is dominated by a few ($\mathcal{N}^5$)-scaling steps:

- the integrals $(ai|\hat{}|bj)$ $(\frac{1}{2}O^2V^2X)$ and $(ai|\bar{}|bj)$ (mO^2V^2X)
- the intermediates $\tilde{Y}_{Q,ci}$ $(mO^2V^2X$ for the real case and $2mO^2V^2X$ for the complex case)

where m is the number of trial vectors, O is the number of occupied orbitals, V is the number of virtual orbitals, and X is the number of auxiliary basis functions (typically $X \approx 3\,N$) and a system without point group symmetry is assumed. The simultaneous transformation of many trial vectors ($m \gg 1$) should thus, in the limit of a large system size for the CPP case, take ≈50% longer than for the (normal) non-CPP case, ≈44% longer for two trial vectors, and ≈40% longer for a single trial vector. Some exemplificative timings for C_{60} are collected in Table IV in Appendix A. The table summarizes the total time per response vector (in min) and the averaged time per vector and per solver iteration when computing the response amplitudes needed to calculate one component of the dipole polarizability of C_{60}, using either the standard or the CPP solver. Three frequency values ω were considered: 0.0 a.u. (static case), 0.07 a.u. (far from resonance), and 0.2 a.u. (close to resonance). For the imaginary frequency γ, only two values were considered: 0.0 and 4.6×10^{-3} a.u. (1000 cm^{-1}). For C_{60}, the lower scaling steps are, in particular, because D_{2h} symmetry was used, not yet negligible. For these steps, the extra costs for the CPP case are lower, and we thus observe for C_{60} overheads for the CPP case of ≈20%. The standard solver is (obviously) more convenient in the static case and at frequencies far from resonance. Close to resonance, the standard solver clearly struggles, and a larger number of iterations are needed for convergence. This effect is smaller with a non-zero gamma.

B. One-photon absorption: C_{60}

The UV spectrum of C_{60} obtained at the CPP-RI-CC2/aug-cc-pVDZ level (all electrons correlated) is shown in Fig. 1. The spectrum is compared with the CPP-KS-TDDFT result of Ref. 16. C_{60} is a prototypical case where the application of the CPP algorithm is particularly advantageous. The molecular point group symmetry of C_{60} is I_h, and the dipole allowed transitions belong to the T_{1u} irrep. If the quantum chemistry code used for the spectral calculations only supports Abelian symmetry, the symmetry descent from I_h to D_{2h} implies that the dipole allowed transitions belong to the same irrep (B_{1u}) as several other forbidden excitations. Thus, straightforward calculation of excitation energies and oscillator strengths results in an exceedingly large number of roots with no intensity to be converged. Moreover, C_{60} is an example for a material with a large number of atoms in a similar chemical situation and, thus, a dense spectrum, which makes it costly to compute the spectrum for a given energy or frequency range in the traditional way. C_{60} already has (at the CC2/aug-cc-pVDZ level) about 500 states below 7 eV (60 of them in B_{1u}). For larger fullerenes, this number will increase, roughly linearly with the number of C atoms. With the CPP approach, on the other hand, the number of points will not increase with the system size.

In the example below, we converged 60 B_{1u} states (D_{2h} point group), which covered an energy range up to 6.90 eV, and only obtained four states with non-zero intensity at ~3.6, ~4.6, ~5.5, and ~6.4 eV, which are shown in Fig. 1 as red vertical sticks. The spectrum computed with our CPP-RI-CC2 and the one from a previously reported CPP-B3LYP study (obtained using the pol-Sadlej [10s6p4d|5s3p2d] basis)[16] also cover the frequency region up to 7 eV and show four peaks of varying intensity. The intensity of the bands is slightly larger in RI-CC2 compared to CPP-B3LYP. The CPP-B3LYP spectrum is blue-shifted by ~0.3 eV with respect to the one obtained with CPP-RI-CC2.

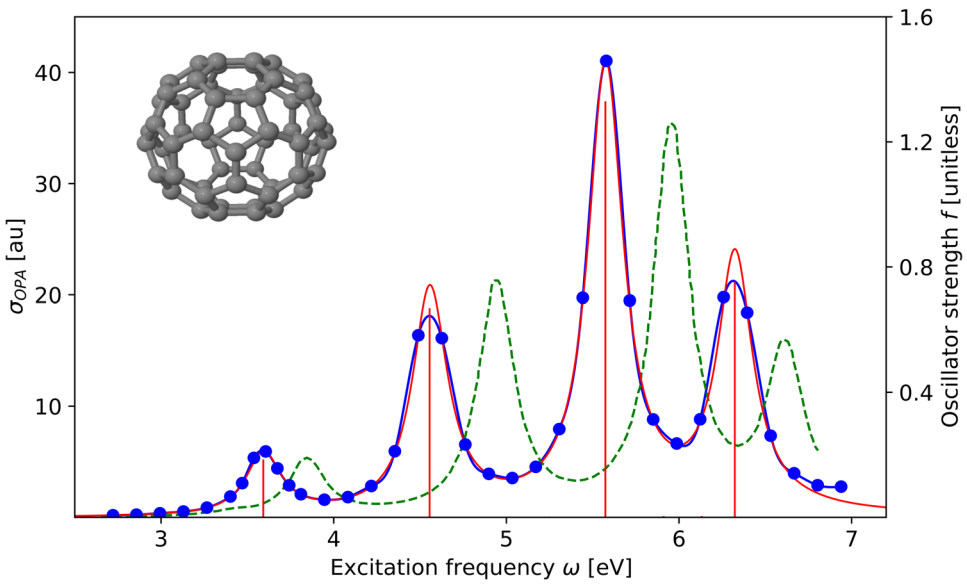

FIG. 1. C_{60}: RI-CC2/aug-cc-pVDZ UV–Vis OPA spectra from standard linear response (red) and CPP (blue) calculations. The red sticks (RI-CC2/aug-cc-pVDZ/frozen core) are the only excitations with non-zero intensity up to 6.9 eV (first 60 B_{1u} roots in the D_{2h} point group). The CPP spectrum shown as a blue line is a cubic spline of the computed CPP grid points. The dashed green line is the CPP-B3LYP/pol-Sadlej spectrum re-digitized from Ref. 53.

C. Electronic circular dichroism: Helicenes

Helicenes are prototypical systems that show chiro-optical activity not because of the presence of chiral centers (e.g., asymmetric carbon atoms), but because of the handedness of their helical structure, also known as axial chirality, as the clockwise and counterclockwise helices are non-superposable. By convention, a left-handed helix is *minus*, (−), and labeled M, whereas a right-handed helix is *plus*, (+), and labeled P. The *n*-helicenes are also a prototypical example of overcrowded aromatic chromophores, and the enantiomers possess a strong optical activity,[56–60] which makes them ideal test systems for our CPP-RI-CC2 computational scheme. ECD spectra of helicenes were theoretically studied before,[61–65] e.g., in 2000 at the TDDFT level by Furche *et al.*[61] and, for 5-helicene and 6-helicene, in 2003 by Köhn[62] at the CC2 level using the aug-cc-pVDZ basis supplemented with center of mass functions. The standard response spectra in the latter study included the lowest 24 and 20 states, respectively. In 2012, a combined theoretical and experimental study on several helicenes was also presented by Nakai, Mori, and Inoue,[65] where the computed ECD spectra were obtained at the RI-CC2 level using the TZVPP basis set and 40 excited states. To illustrate the CPP approach, we here extend the RI-CC2 studies of Refs. 62 and 65 by investigating the penta-helicene, hexa-helicene, and hepta-helicene using the larger aug-cc-pVTZ basis set. Experimental spectra were re-digitized from the original references and are shown together with the calculated ones.

The ECD spectra of (−)-5-helicene are shown in Fig. 2. By converging 40 excited states, we could obtain the standard (broadened) linear response spectrum up to approximately 6.3 eV. Experimental[56,60,65] and CPP spectra cover the frequency range up to 6.2 and 7.7 eV, respectively. One[56,60] of the shown experimental spectra was recorded in *iso*-octane. Note that we re-digitized the experimental spectrum reported in Fig. 2 of Ref. 56. According to the authors,[56] this experimental spectrum was taken from the work of Goedicke and Stegemeyer,[60] even though no image of the spectrum is actually given by Goedicke and Stegemeyer, who only report individual values of $\Delta\varepsilon$ at given wavelengths. Spectral data from both articles are presented as a green continuum line and triangles in Fig. 2. We observe small inconsistencies at around 4 and 5.5 eV between the spectrum re-digitized from Ref. 56 and the spectral points taken from Ref. 60 (green triangles). The experimental spectrum from Ref. 65, recorded in 98:2 *n*-hexane/2-propanol, is shown as a dashed green line.

The stick spectrum starts with one positive peak of symmetry A and very low intensity (marked by an arrow). Roughly in the same region, the experiment[56,60] shows two low intensity positive features (~50 times weaker than the rest of the spectrum).[56,60] The CPP and the Lorentzian broadened spectra are practically indistinguishable up to around 5.85 eV, where differences start to emerge, as individual excitations may be missing in the latter. The computed and experimental spectra have similar features: two negative bands, one at around 4 eV and one just above 5 eV, two positive overlapping bands at around 4.5–4.7 eV, and a feature-rich positive band, starting in between 5 and 6 eV, clearly due to a large number of transitions. The computed spectra (*in vacuo*) are slightly blue-shifted and of lower intensity compared to the experimental data in *iso*-octane.[60]

The ECD spectra for (−)-6-helicene are presented in Fig. 3. Note that the experimental measurement from Ref. 57 was carried out in methanol on the P structure, so we have reversed its sign when comparing it in Fig. 3 with the spectra computed for the M enantiomer (solid green line). The experimental CD spectrum recorded in acetonitrile from Ref. 65 is also shown as a dashed green line.

As the system size increases, it becomes progressively more challenging to converge the standard response spectra. For 6-helicene, the first 20 excited states were explicitly calculated. This, however, only covers the region up to 5.2 eV. The CPP spectrum was computed up to 7.3 eV. The CPP and broadened standard response

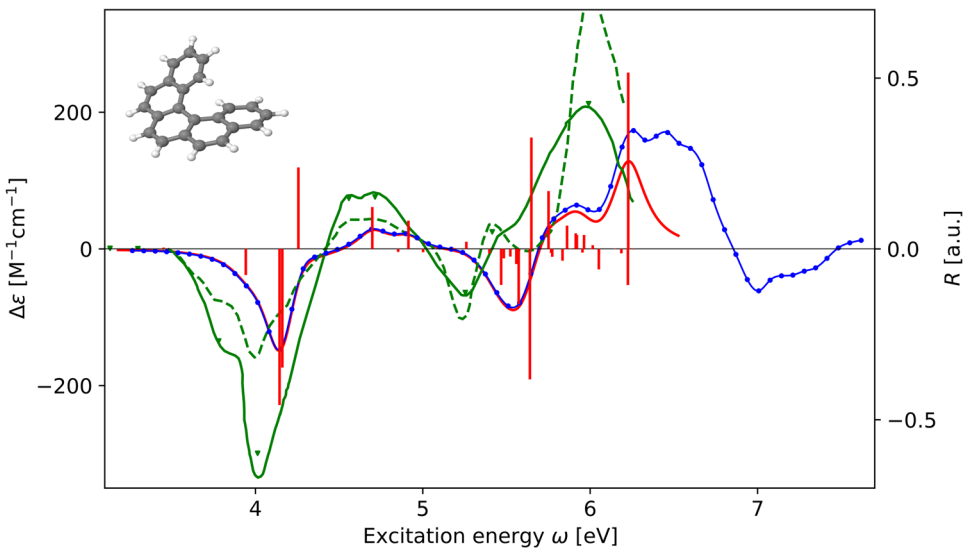

FIG. 2. (−)-5-Helicene (M): (frozen-core) RI-CC2/aug-cc-pVTZ ECD spectra from resonant linear response and CPP calculations. The individual excitation energies and rotatory strengths and their Lorentzian broadened spectrum are reported in red. The blue circles are the CPP points, and the blue line is a cubic spline of the CPP points. The solid green line is the experimental spectrum re-digitized from Ref. 56, which is (supposedly) derived from the measurement in *iso*-octane in Ref. 60 (green triangles). The dashed green line is the experimental spectrum re-digitized from Ref. 65, recorded in 98:2 *n*-hexane/2-propanol.

spectra start to differ at around 5.2 eV. Indeed, the intensity of the strongest positive peak predicted by the CPP spectrum is slightly lower than the one obtained from broadening the individual excitation energies and rotatory strengths, probably the effect of the broad negative band, located in between 5.5 eV and 5.7 eV, clearly not present in the broadened spectrum as the corresponding excited states were not computed.

All in all, as for 5-helicene, the computed and experimental spectra of 6-helicene have rather similar features: a relatively strong negative peak at around 3.8 eV and two (partly overlapping) positive peaks in between 4.8 and 5.3 eV, followed by a bisignate band in between 5.5 and 6.3 eV. The computed first negative peak at 3.9 eV is marginally blue-shifted with respect to the experimental band. The band intensities in the simulated spectrum are only slightly larger than the corresponding ones in the experimental spectrum recorded in methanol. The lowest-energy band is practically overlapping with the same band from the experimental measurement in acetonitrile.[65]

The ECD spectra for (+)-7-helicene are presented in Fig. 4. The mirror image of the experimental spectrum of (−)-7-helicene, recorded in ethanol by Brickell *et al.*,[58] is shown as a solid green line in Fig. 4. The experimental spectrum in chloroform reported by Nakai, Mori, and Inoue,[65] originally taken from the study of Martin and Marchant,[66] is also shown as a dashed line. The CPP spectrum

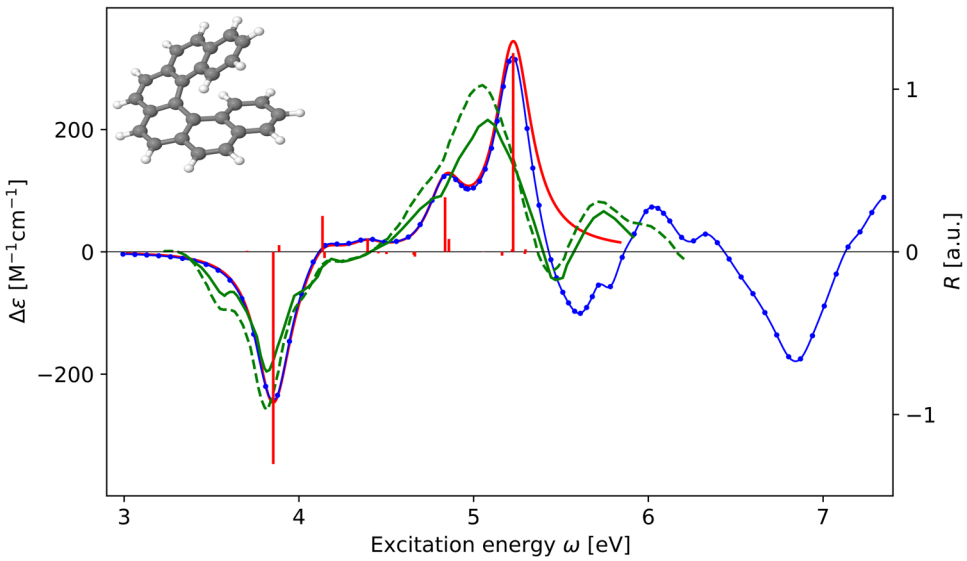

FIG. 3. (−)-6-Helicene (M): (frozen-core) RI-CC2/aug-cc-pVTZ ECD spectra from standard linear response and CPP calculations. The individual excitation energies and rotatory strengths and their Lorentzian broadened spectrum are reported in red. The blue circles are the CPP points, and the blue line is a cubic spline through the CPP points. A mirror image of the experimental spectrum of (+)-6-helicene (P) from Ref. 57, recorded in methanol, is shown as a solid green line. A dashed green line shows the experimental spectrum recorded in acetonitrile, re-digitized from Ref. 65.

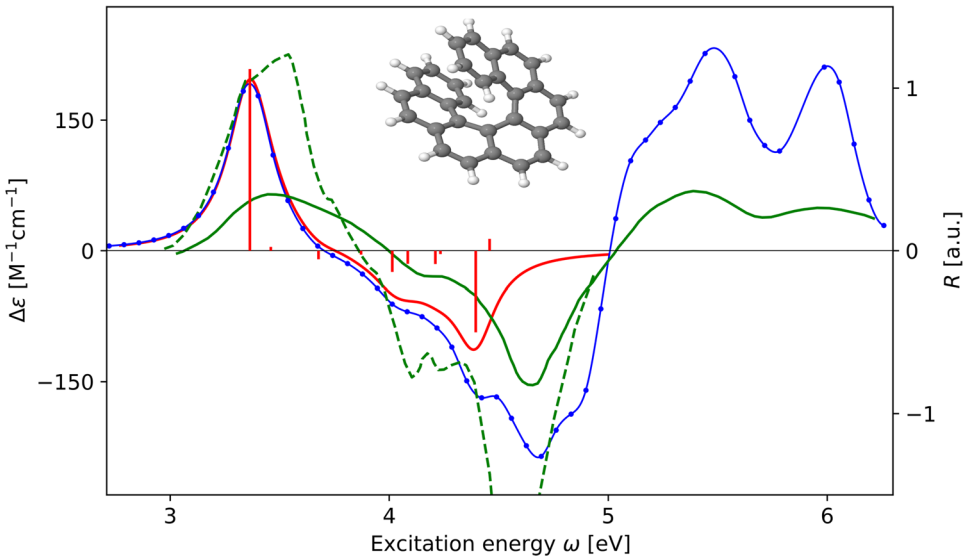

FIG. 4. (+)-7-Helicene (P): (frozen-core) RI-CC2/aug-cc-pVTZ ECD spectra from resonant linear response and CPP calculations. The individual excitation energies and rotatory strengths and their Lorentzian broadened spectrum are reported in red. The blue circles are the CPP points, and the blue line is a cubic spline through the CPP points. A mirror image of the experimental spectrum of (−)-7-helicene (M) from Ref. 58, recorded in ethanol, is shown as a solid green line. The experimental spectrum in chloroform[65,66] is given as a dashed green line.

was obtained up to 6.25 eV and shows a well-separated positive peak between 3 and 3.7 eV; a feature-rich negative band between 3.7 and 5 eV, clearly with contributions from several transitions of different intensity and with maximum at 4.7 eV; and two positive peaks at 5.44 and 5.99 eV, respectively. All peaks are of comparable intensity. Not surprisingly, with the increase in complexity of the system, our ability to solve for the individual excited state energies and rotatory strengths deteriorates. Indeed, for 7-helicene, we only succeeded in converging 12 states, which cover the region up to 4.5 eV, thus only reproducing the first (positive) peak and half of the negative broad band.

Despite the different environments, the experimental spectral profiles are, as in the previous two cases, quite similar to the computed one, with a broad positive band at lower energy, a structured negative one in the intermediate region, and two positive bands in the upper frequency region. The experimental intensity of the spectrum in ethanol is, on the other hand, roughly two times lower, whereas the one in chloroform is more intense, in particular in the intermediate frequency region.

D. The C_6 dispersion coefficients

In Table II, we present the C_6 dispersion coefficients for the dimers of a set of ten organic molecules. In Table III, the results for six different fullerenes are collected.

The RI-CC2 values for the C_6 coefficients of the organic molecules are in line with the results of a previous theoretical study at the ADC(2)/Sadlej-pVTZ level.[15] The percentage difference

TABLE II. RI-CC2/aug-cc-pVTZ C_6 dispersion coefficients (a.u.) of the dimers of ten organic molecules and comparison with previous theoretical results, obtained at the ADC(2)/Sadlej-pVTZ[15] and CCSD/Sadlej-pVTZ[15] levels of theory, and with DOSD results. $\%\Delta C_6^{\mathrm{ADC(2)}} = 100 \times (C_6^{\mathrm{CC2}} - C_6^{\mathrm{ADC(2)}})/C_6^{\mathrm{ADC(2)}}$, $\%\Delta C_6^{\mathrm{DOSD}} = 100 \times (C_6^{\mathrm{CC2}} - C_6^{\mathrm{DOSD}})/C_6^{\mathrm{DOSD}}$.

Molecules	RI-CC2	ADC(2)[15]	$\%\Delta C_6^{\mathrm{ADC(2)}}$	CCSD[15]	DOSD	$\%\Delta C_6^{\mathrm{DOSD}}$
Acetaldehyde	432.8	434.3	−0.4	407.2	401.8[67]	7.7
Acetone	834.0	832.0	0.24	787.4	794.5[67]	5.0
Benzene	1874	1926	−2.7	1786	1723[68]	8.8
Butane	1285	1263	1.7	1224	1268[69]	1.3
Ethane	374.5	365.9	2.4	357.3	381.8[69]	−1.9
Ethene	305.9	299.8	2.03	287.3	300.2[70]	1.9
Formaldehyde	154.0	157.6	−2.3	144.8	165.2[67]	−6.8
Methane	126.3	122.7	2.9	120.7	129.6[71]	−2.5
Pentane	1950	1918	1.7	1855	1905[69]	2.4
Propane	759.9	745.1	2.0	724.2	768.1[69]	−1.1

TABLE III. RI-CC2 C_6 dispersion coefficients [a.u. $\times 10^{-3}$] for a set of fullerene dimers and comparison with previous literature results.[53,72]

Molecule	RI-CC2/ cc-pVDZ	B3LYP/ pol-Sadlej[53]	CAM-B3LYP/ pol-Sadlej[53]	TD-HF/ pol-Sadlej[53]	DOSD[72]
C_{60}	97.08[a]	100.8	98.8	100.1	100.3
C_{70}	141.4	143.0	139.8	141.6	
C_{78}	179.1	180.0	176.1	178.2	
C_{80}	191.3	193.1	189.4	192.5	
C_{82}	197.9	199.1	194.8	196.8	
C_{84}	208.6	209.8	205.4	207.7	

[a]117.7 × 10^3 (aug-cc-pVDZ); At MP2 geometry, 96.00 × 10^3 (cc-pVDZ); 116.3 × 10^3 (aug-cc-pVDZ); 115.4 × 10^3 (aug-cc-pVTZ).

between CC2 and ADC(2) values varies between −2.7% (benzene) and +2.9% (methane). The smallest differences between the two methods are observed for acetaldehyde and acetone. Note, however, that we did not use the same basis set in our CC2 calculations as used in the ADC(2) study. Both RI-CC2 and ADC(2) results are systematically larger than corresponding CCSD/Sadlej-pVTZ results from the literature,[15] which were obtained using a Lanczos-based implementation of the polarizability at imaginary frequencies[9] and a moderate chain length. We also compare our CC2 values to estimates from the literature obtained using the dipole oscillator strength distribution (DOSD) approach.[72] In the DOSD approach, the C_6 coefficients are derived from the dipole oscillator strength distributions constructed from theoretical and experimental photoabsorption cross sections, combined with constraints provided by the Kuhn–Reiche–Thomas sum rule and molar refractivity data. In this case, the differences in percentage range from ∼−1% (propane) to +9% (benzene).

The CC2/cc-pVDZ results for the C_6 coefficients of the fullerenes, see Table III, are compared to literature results at the CAM-B3LYP, B3LYP, and TD-HF levels of theory,[53] obtained with the pol-Sadlej basis set. We note that our basis set is on the small side, so our results are probably not fully converged. Indeed, adding one set of augmented functions increased the coefficient for C_{60} to 117.7 × 10^3. At the MP2 geometry used in the OPA calculations, the C_6 coefficient of C_{60} changes from 96.00 × 10^3 (cc-pVDZ) to 116.3 × 10^3 (aug-cc-pVDZ) to 115.4 × 10^3 (aug-cc-pVTZ). A reference value, obtained using the DOSD approach, is available for C_{60}.[72] As already commented upon in Ref. 53, the TD-HF/pol-Sadlej result is the closest to the DOSD value, but good agreement is probably fortuitous.

In Fig. 5, the C_6 coefficients are plotted as a function of the number N of carbon atoms in the considered fullerenes. In the inset, a plot of the ratios $C_6(C_N)/C_6(C_{60})$ vs $N/60$ is given. Figure 6 reports the base-10 logarithm of C_6 coefficients as a function of $\log N$. The

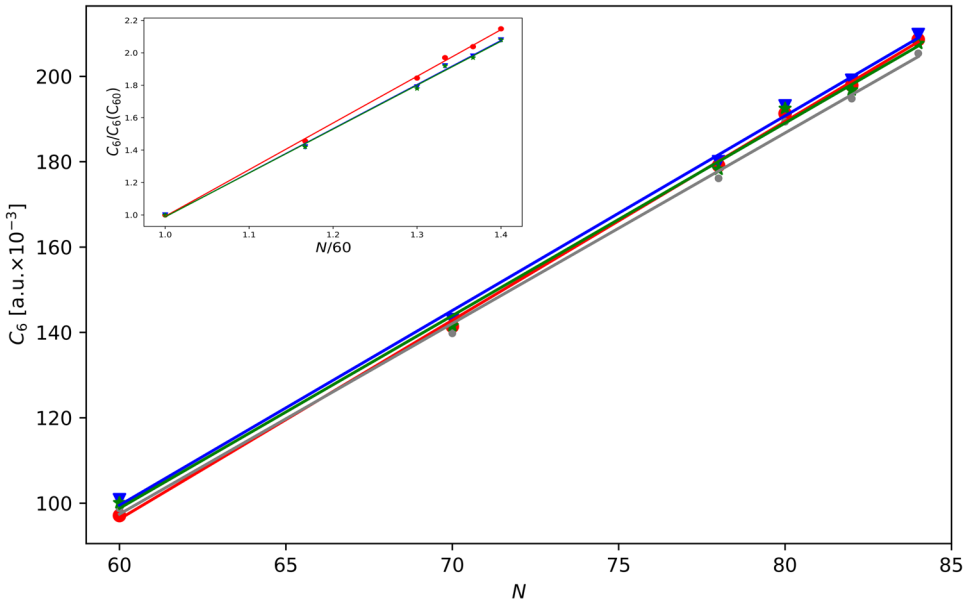

FIG. 5. C_6 coefficients (a.u. × 10^{-3}) of six fullerenes as a function of the number of carbon atoms N, plotted for four different electronic structure methods. The inset shows the ratios $C_6(C_N)/C_6(C_{60})$ vs $N/60$. Red: RI-CC2; blue: B3LYP; gray: CAMB3LYP; green: TD-HF results. The lines are linear regressions of the C_6 points. The regression coefficients for the lines in the main panel are r = 0.9995 (RI-CC2), r = 0.9986 (HF), r = 0.9991 (B3LYP), and r = 0.9989 (CAM-B3LYP). Those of the lines in the inset are r = 0.9995 (RI-CC2), r = 0.9988 (HF), r = 0.9991 (B3LYP), and r = 0.9988 (CAM-B3LYP).

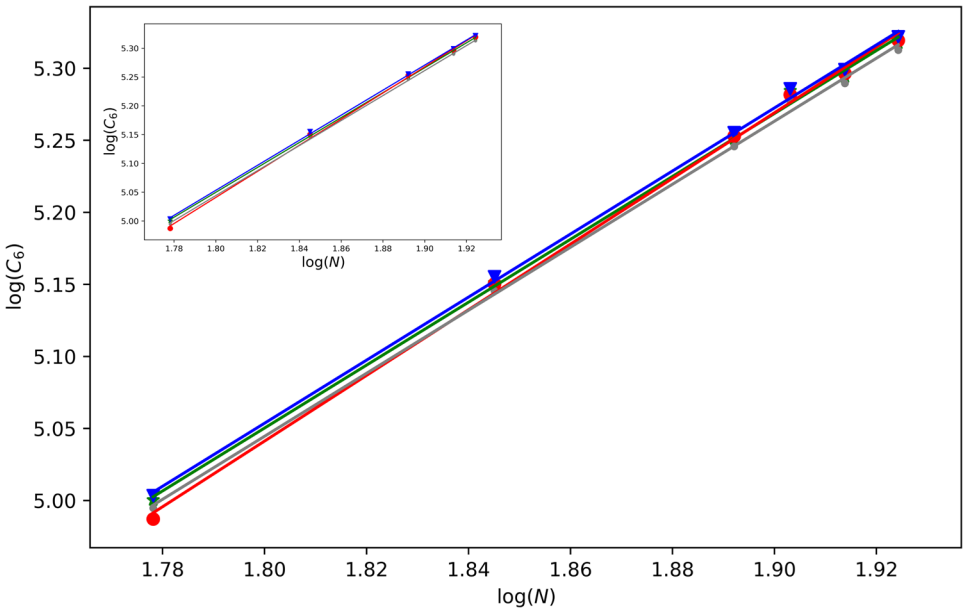

FIG. 6. Base-10 logarithm of the C_6 coefficients of six fullerenes as a function of log N, for four different electronic structure methods. Red: RI-CC2 (this work, r = 0.9992); blue: B3LYP (r = 0.9994); gray: CAMB3LYP (r = 0.9994); green: TD-HF (r = 0.9991) results. The inset shows the data without consideration of C_{80}, which slightly improves the linear regression coefficient: r = 0.9998 for HF, r = 0.9998 for B3LYP, r = 0.9998 for CAM-B3LYP, and r = 0.9994 for RI-CC2.

latter figure is used to determine the exponent η at the RI-CC2 level of the ansatz $C_6 \propto N^{\eta}$, as also reported by Kauczor, Norman, and Saidi.[53] Kauczor, Norman, and Saidi[53] found that the C_6 coefficients were non-additive and scaled roughly as $N^{2.2}$ for the three methods they considered. The exponent for the C_6 power-dependence on N was, therefore, much smaller than the values predicted based on a classical-metallic spherical-shell approximation of the fullerenes (≈2.75).[73] In a later study, some of the same authors[74] proposed a model based on classical electrodynamics that yielded $C_6 \propto N^{2.8}$. Our results at the CC2 level, based on small-size fullerenes, give η = 2.3, i.e., only marginally larger than the HF/DFT estimates of Kauczor, Norman, and Saidi. Removing C_{80} from the series slightly improves the linear regression coefficients but does not significantly change the value of η.

V. CONCLUSIONS

We have presented an implementation of a damped linear response solver and of the damped linear response function within the resolution-of-identity CC2 method in Turbomole.[31] The LR-CPP-RI-CC2 approach allows us to directly compute, e.g., ECD and OPA spectra of systems with a high density of excited states, where a standard response approach is hardly or not applicable. The combination of the RI approximation with a partitioned formulation that avoids the storage and I/O of four-index two-electron integrals and double excitation amplitudes (employing a Laplace transformation of orbital energy denominators) together with an OpenMP parallelization makes the LR-CPP-RI-CC2 approach applicable to molecular systems as large as fullerenes and helicenes.

Examples of application of the approach included the OPA spectra of C_{60}, the ECD spectra of n-helicenes (n = 5, 6, 7), and the C_6 dispersion coefficients for a sample of organic molecules and fullerenes.

The CPP solver for RI-CC2 is also a fundamental stepping stone for the implementation of higher-order response properties in a RI-CC2 CPP framework, e.g., RIXS and MCD, as well as for the extension to excited state properties.

SUPPLEMENTARY MATERIAL

The following additional information is found in the supplementary material: Cartesian coordinates of all studied molecules and raw spectral data (excitation energies and oscillator/rotatory strengths) for C_{60}, 5-helicene, 6-helicene, and 7-helicene.

ACKNOWLEDGMENTS

We thank Dr. Thomas Fransson (University of Heidelberg) and Professor Wissam Saidi (University of Pittsburgh) for sending us the Cartesian coordinates of the molecular systems considered for the C_6 coefficients. D.A.F. thanks Dr. Rasmus Faber (DTU) and Dr. Alireza Marefat Khah (RUB) for valuable discussions. D.A.F. and S.C. acknowledge the financial support from the Marie Skłodowska-Curie European Training Network "COSINE-COmputational Spectroscopy In Natural sciences and Engineering" under Grant Agreement No. 765739. S.C. acknowledges Independent Research Fund Denmark—Natural Sciences, Research Project 2, Grant No. 7014-00258B. C.H. acknowledges the financial support by DFG through Grant No. HA 2588/8.

APPENDIX A: TIMINGS

Table IV presents computational timings (t, min) to converge one response amplitude for the calculation of one component of the

TABLE IV. Computational timings (t, min) to converge one response amplitude for the calculation of one component of the dipole polarizability of C_{60} using the damped and the standard linear response solvers. N_{iter} is the number of iterations and N_{vect} is the number of response vectors timings are normalized to one response vector. All calculations were performed using Central DTU HPC Cluster, on the node "Lenovo ThinkSystem SD530" with the following configuration: 2 x Intel Xeon Gold 6126 (12 cores, 2.60 GHz); 12 × 192 GB/11 × 384 GB/1 × 768 GB memory; 480 GB SSD. The convergence threshold was 10^{-6}.

Solver	Total t/vect	N_{iter}	N_{vect}	$t/(\text{iter}\cdot\text{vect})$
Standard ($\omega = 0.00$ a.u.)	28.0	10	1	2.80
Standard ($\omega = 0.07$ a.u.)	24.6	14	2	1.76
Standard ($\omega = 0.20$ a.u.)	119.7	74	2	1.62
Damped ($\omega = 0.00$ a.u., $\gamma = 0.0$ a.u.)	32.83	9	1	3.65
Damped ($\omega = 0.07$ a.u., $\gamma = 0.0$ a.u.)	34.50	13	2	2.65
Damped ($\omega = 0.20$ a.u., $\gamma = 0.0$ a.u.)	109.7	54	2	2.03
Damped ($\omega = 0.20$ a.u., $\gamma = 4.60 \times 10^{-3}$ a.u.)	84.56	43	4	1.97

dipole polarizability of C_{60} using the damped and the standard linear response solvers.

APPENDIX B: ADDITIONAL DEFINITIONS

- T_1-similarity-transformed MO coefficients:

$$\mathbf{\Lambda}^p = \mathbf{C}(\mathbf{1} - \mathbf{t}_1^T), \quad \mathbf{\Lambda}^h = \mathbf{C}(\mathbf{1} + \mathbf{t}_1).$$

- T_1-similarity-transformed one-electron integrals:

$$\hat{h}^x_{pq} = \sum_{\alpha\beta} \Lambda^p_{\alpha p} \Lambda^h_{\beta q} h^x_{\alpha\beta}.$$

- T_1-similarity-transformed two-electron integrals:

$$(pq|\hat{rq}) = \sum_{\alpha\beta\gamma\delta} \Lambda^p_{\alpha p} \Lambda^h_{\beta q} \Lambda^p_{\gamma r} \Lambda^h_{\delta s} (\alpha\beta|\gamma\delta).$$

- The elements of $\hat{\mathbf{F}}$ are defined as the elements of the usual Fock matrix, but evaluated with T_1-similarity-transformed one-electron and two-electron integrals.
- One-index transformed $\check{\mathbf{\Lambda}}^p$ and $\check{\mathbf{\Lambda}}^h$ matrices:

$$\check{\Lambda}^p_{\beta i} = \sum_a \Lambda^p_{\beta a} \bar{t}_{ia} \quad \text{and} \quad \check{\Lambda}^h_{\beta a} = -\sum_i \Lambda^h_{\beta i} \bar{t}_{ia}.$$

- t^x-dressed one-index transformed $\bar{\mathbf{\Lambda}}^{p,x}$ and $\bar{\mathbf{\Lambda}}^{h,x}$ matrices (*):

$$\bar{\Lambda}^{p,x}_{\beta a} = -\sum_i C_{\beta i} t^x_{ai} \quad \text{and} \quad \bar{\Lambda}^{h,x}_{\beta i} = \sum_a C_{\beta a} t^x_{ai}.$$

- Barred one-electron and three-center and four-center two-electron integrals (*):

$$\bar{h}^x_{pq} = \sum_{\alpha\beta} \left(\bar{\Lambda}^{p,x}_{\alpha p} \Lambda^h_{\beta q} + \Lambda^p_{\alpha p} \bar{\Lambda}^{h,x}_{\beta q} \right) h_{\alpha\beta},$$

$$\bar{B}^x_{Q,pq} = \sum_P (pq|\bar{P}) V^{-\frac{1}{2}}_{PQ}$$

$$= \sum_{\alpha\beta} \left(\bar{\Lambda}^{p,x}_{\alpha p} \Lambda^h_{\beta q} + \Lambda^p_{\alpha p} \bar{\Lambda}^{h,x}_{\beta q} \right) \sum_P (\alpha\beta|P) V^{-\frac{1}{2}}_{PQ},$$

$$(pq|\bar{rs})^x = \hat{P}^{pr}_{qs} \sum_{\alpha\beta\gamma\delta} \left(\bar{\Lambda}^{p,x}_{\alpha p} \Lambda^h_{\beta q} + \Lambda^p_{\alpha p} \bar{\Lambda}^{h,x}_{\beta q} \right) \Lambda^p_{\gamma r} \Lambda^h_{\delta s} (\alpha\beta|\gamma\delta).$$

Here, it is understood that $\bar{\Lambda}^{p,x}_{\alpha p}$ vanishes if p is an occupied index and $\bar{\Lambda}^{h,x}_{\beta q}$ vanishes if q is a virtual index.

- Barred Fock matrices and E intermediates (*):

$$\bar{F}^x_{ia} = \sum_{ck} [2(ia|kc) - (ic|ka)] t^x_{ck},$$

$$\bar{F}^x_{ab} = -\sum_j t^x_{aj} \hat{F}_{jb} + \sum_{ck} [2(ab|kc) - (ac|kb)] t^x_{ck},$$

$$\bar{F}^x_{ij} = +\sum_b \hat{F}_{jb} t^x_{bi} + \sum_{ck} [2(ij|kc) - (ic|kj)] t^x_{ck},$$

$$\bar{E}^{x,2}_{ij} = \bar{F}^x_{ij} + \sum_{cdk} \left[2t^{x,jk}_{cd} - t^{x,jk}_{dc} \right] (kd|ic),$$

$$\bar{E}^{x,2}_{ba} = \bar{F}^x_{ba} + \sum_{dkl} \left[2t^{x,kl}_{bd} - t^{x,kl}_{db} \right] (ld|ka).$$

An asterisk (*) indicates that the respective intermediates depend linearly on the complex response amplitude t^x and have been generalized to the CPP case such that their real and imaginary parts are evaluated, respectively, with the real and imaginary parts of t^x.

ALGORITHM 1. Main steps in the evaluation of the F-matrix contraction terms. An asterisk (*) indicates the terms that have been generalized to the CPP case (complex).

- Compute $\check{Y}_{Q,ck} = \sum_{dj} \bar{t}^{jk}_{dc} \hat{B}_{Q,dj}$ (standard code)
- Compute $\bar{F}^x_{ia}$, $\bar{E}^{x,1}_{ab}$, $\bar{E}^{x,2}_{ij}$, $\bar{B}^x_{Q,bj}$, $\bar{B}^x_{Q,ij}$, C^x_{ck}, $Y^x_{Q,ai}$ (*)
- Compute dressed integrals $\check{B}^x_{Q,jb} = -\sum_{ck}\left(\bar{t}_{jc}t^x_{ck}B_{Q,kb} + t^x_{ck}\bar{t}_{kb}B_{Q,jc}\right)$ (*) [Eq. (85)]
- Compute $\sigma^{0,x}_{ia} = 2\bar{F}^x_{ia}$, $\sigma^{JG,x}_{ia}$ and $\sigma^{JH,x}_{ia}$ (*)
- Compute intermediates:
  - $-\check{\Lambda}^p_{\beta i}$, $\check{\Lambda}^h_{\beta a}$ and $\check{B}_{Q,ia} = \sum_{\alpha\beta p}\Lambda^h_{\alpha a}\check{\Lambda}^p_{\beta i}(\alpha\beta|P)V^{-1/2}_{PQ} - \sum_k \hat{B}_{Q,ik}\bar{t}_{ka}$ (standard code)
  - $-\bar{t}^{ij}_{ab} = (2-\hat{P}_{ij})\hat{P}^{ij}_{ab}\left(\sum_Q \check{B}_{Q,ai}B_{Q,jb} + \bar{t}_{ia}\hat{F}_{jb}\right)/(\varepsilon_i - \varepsilon_a + \varepsilon_j - \varepsilon_b)$ (standard code)
  - $-\check{Y}^x_{Q,ia} = \sum_{bj}\bar{t}^{ij}_{ab}\bar{B}^x_{Q,jb}$ (*)
  - $-m^x_Q = \sum_{ck} B_{Q,ck}C^x_{ck}$ and $M^x_{Q,ik} = \sum_c B_{Q,ic}C^x_{ck}$ (*)
  - $-\check{t}^x_Q = \sum_{jb}\bar{B}^x_{Q,bj}\bar{t}_{jb}$ (*)
  - $-\check{\Gamma}^x_{Q,\beta i} = \sum_{Pa}\left(\check{Y}^x_{P,ia} - \sum_j \bar{t}_{ja}\bar{B}^x_{P,ij}\right)V^{-1/2}_{PQ}\Lambda^p_{\beta a} - \sum_{Pk}M^x_{P,ik}V^{-1/2}_{PQ}\Lambda^p_{\beta k} + 2\sum_P\left(m^x_P + \check{t}^x_P\right)V^{-1/2}_{PQ}\Lambda^p_{\beta i}$ (*)
  - $-\sigma^{IJ'_{12}F_1,x}_{i\alpha} = \sum_{Q\beta}\check{\Gamma}^x_{Q,\beta i}(Q|\beta\alpha)$
- Compute $\sigma^{IJ'_{12}F_1,x}_{ia} = \sum_\alpha \sigma^{IJ'_{12}F_1}_{i\alpha}C_{\alpha a}$ ($\sigma^{I,x}_{ia}$ + first term of $\sigma^{F,x}_{ia}$ + first and second term of $\sigma^{J',x}_{ia}$) (*)
- Compute $\sigma^{F_3,x}_{ia} = -\sum_{lQ}\check{Y}^x_{Q,al}\hat{B}_{Q,il}$ (third term of $\sigma^{F,x}_{ia}$) (*)
- Compute intermediate $\check{\Gamma}^{x''}_{Q,i\beta} = \sum_{Pd}\left(\check{Y}_{P,id} - \sum_j \hat{B}_{P,ij}\bar{t}_{jd}\right)\bar{\Lambda}^{p,x}_{\beta d}V^{-1/2}_{PQ}$ (*)
- Compute $\sigma^{F_2J'_3,x}_{i\alpha} = \sum_{Q\beta}\check{\Gamma}^{x''}_{Q,i\beta}(Q|\beta\alpha)$ (*)
- Compute $\sigma^{F_2J'_3,x}_{ia} = \sum_\alpha \sigma^{F_2J_3,x}_{i\alpha}C_{\alpha a}$ (second term of $\sigma^{F,x}_{ia}$+ third term of $\sigma^{J',x}_{ia}$) (*)
- Calculate $\sigma^{F_4,x}_{ia} = -\sum_{lQ}\check{Y}_{Q,al}\bar{B}^x_{Q,il}$ (*)
- Contract with single amplitudes and add the doubles contributions

$$Ft^x t^y = \sum_{ai}\sigma^x_{ia}t^y_{ai} + \sum_{ai}\bar{F}^x_{ia}C^y_{ai} + \sum_{Q,bj}\check{B}^x_{Q,jb}Y^y_{Q,bj}\ (*)$$

DATA AVAILABILITY

The data that support the findings of this study are available within this article and its supplementary material.

REFERENCES

[1] K. Kristensen, J. Kauczor, T. Kjærgaard, and P. Jørgensen, J. Chem. Phys. **131**, 044112 (2009).
[2] P. Norman, D. M. Bishop, H. J. A. Jensen, and J. Oddershede, J. Chem. Phys. **115**, 10323 (2001).
[3] P. Norman, D. M. Bishop, H. J. A. Jensen, and J. Oddershede, J. Chem. Phys. **123**, 194103 (2005).
[4] L. Jensen, J. Autschbach, and G. C. Schatz, J. Chem. Phys. **122**, 224115 (2005).
[5] U. Ekström, P. Norman, V. Carravetta, and H. Ågren, Phys. Rev. Lett. **97**, 143001 (2006).
[6] U. Ekström and P. Norman, Phys. Rev. A **74**, 042722 (2006).
[7] T. Fahleson, H. Ågren, and P. Norman, J. Phys. Chem. Lett. **7**, 1991 (2016).
[8] S. Coriani, T. Fransson, O. Christiansen, and P. Norman, J. Chem. Theory Comput. **8**, 1616 (2012).
[9] S. Coriani, O. Christiansen, T. Fransson, and P. Norman, Phys. Rev. A **85**, 022507 (2012).
[10] R. Faber and S. Coriani, J. Chem. Theory Comput. **15**, 520 (2019).
[11] P. Norman, Phys. Chem. Chem. Phys. **13**, 20519 (2011).
[12] K. Kristensen, J. Kauczor, A. J. Thorvaldsen, P. Jørgensen, T. Kjærgaard, and A. Rizzo, J. Chem. Phys. **134**, 214104 (2011).
[13] D. R. Rehn, A. Dreuw, and P. Norman, J. Chem. Theory Comput. **13**, 5552 (2017).
[14] A. Jiemchooroj, B. E. Sernelius, and P. Norman, Phys. Rev. A **69**, 044701 (2004).
[15] T. Fransson, D. R. Rehn, A. Dreuw, and P. Norman, J. Chem. Phys. **146**, 094301 (2017).
[16] J. Kauczor and P. Norman, J. Chem. Theory Comput. **10**, 2449 (2014).
[17] M. Scheurer, T. Fransson, P. Norman, A. Dreuw, and D. R. Rehn, J. Chem. Phys. **153**, 074112 (2020).
[18] J. Kauczor, P. Norman, O. Christiansen, and S. Coriani, J. Chem. Phys. **139**, 211102 (2013).
[19] P. Reinholdt, M. S. Nørby, and J. Kongsted, J. Chem. Theory Comput. **14**, 6391 (2018).
[20] M. S. Nørby, S. Coriani, and J. Kongsted, Theor. Chim. Acta **137**, 49 (2018).
[21] T. Fransson, D. Burdakova, and P. Norman, Phys. Chem. Chem. Phys. **18**, 13591 (2016).

[22]L. Konecny, M. Repisky, K. Ruud, and S. Komorovsky, J. Chem. Phys. **151**, 194112 (2019).
[23]A. Jiemchooroj and P. Norman, J. Chem. Phys. **126**, 134102 (2007).
[24]R. Faber and S. Coriani, Phys. Chem. Chem. Phys. **22**, 2642 (2020).
[25]H. Solheim, K. Ruud, S. Coriani, and P. Norman, J. Chem. Phys. **128**, 094103 (2008).
[26]T. Fahleson, J. Kauczor, P. Norman, F. Santoro, R. Improta, and S. Coriani, J. Chem. Phys. **119**, 005476 (2015).
[27]J. Vaara, A. Rizzo, J. Kauczor, P. Norman, and S. Coriani, J. Chem. Phys. **140**, 134103 (2014).
[28]J. Cukras, J. Kauczor, P. Norman, A. Rizzo, G. L. J. A. Rikken, and S. Coriani, Phys. Chem. Chem. Phys. **18**, 13267 (2016).
[29]K. D. Nanda, M. L. Vidal, R. Faber, S. Coriani, and A. I. Krylov, Phys. Chem. Chem. Phys. **22**, 2629 (2020).
[30]F. Furche, R. Ahlrichs, C. Hättig, W. Klopper, M. Sierka, and F. Weigend, Wiley Interdiscip. Rev.: Comput. Mol. Sci. **4**, 91 (2014).
[31]S. G. Balasubramani, G. P. Chen, S. Coriani, M. Diedenhofen, M. S. Frank, Y. J. Franzke, F. Furche, R. Grotjahn, M. E. Harding, C. Hättig, A. Hellweg, B. Helmich-Paris, C. Holzer, U. Huniar, M. Kaupp, A. Marefat Khah, S. Karbalaei Khani, T. Müller, F. Mack, B. D. Nguyen, S. M. Parker, E. Perlt, D. Rappoport, K. Reiter, S. Roy, M. Rückert, G. Schmitz, M. Sierka, E. Tapavicza, D. P. Tew, C. van Wüllen, V. K. Voora, F. Weigend, A. Wodyński, and J. M. Yu, J. Chem. Phys. **152**, 184107 (2020).
[32]O. Christiansen, P. Jørgensen, and C. Hättig, Int. J. Quantum Chem. **68**, 1 (1998).
[33]D. H. Friese, N. O. C. Winter, P. Balzerowski, R. Schwan, and C. Hättig, J. Chem. Phys. **136**, 174106 (2012).
[34]R. Faber, S. Ghidinelli, C. Hättig, and S. Coriani, J. Chem. Phys. **153**, 114105 (2020).
[35]I. Warnke and F. Furche, Wiley Interdiscip. Rev.: Comput. Mol. Sci. **2**, 150 (2012).
[36]T. B. Pedersen, H. Koch, L. Boman, and A. M. J. Sánchez de Merás, Chem. Phys. Lett. **393**, 319 (2004).
[37]D. H. Friese and C. Hättig, Phys. Chem. Chem. Phys. **16**, 5942 (2014).
[38]S. Grimme, J. Comput. Chem. **27**, 1787 (2006).
[39]A. Tkatchenko and M. Scheffler, Phys. Rev. Lett. **102**, 073005 (2009).
[40]S. Grimme, J. Antony, S. Ehrlich, and H. Krieg, J. Chem. Phys. **132**, 154104 (2010).
[41]O. Christiansen, H. Koch, and P. Jørgensen, Chem. Phys. Lett. **243**, 409 (1995).
[42]C. Hättig and F. Weigend, J. Chem. Phys. **113**, 5154 (2000).
[43]C. Hättig and A. Köhn, J. Chem. Phys. **117**, 6939 (2002).
[44]C. Hättig, J. Chem. Phys. **118**, 7751 (2003).
[45]O. Vahtras, J. Almlöf, and M. W. Feyereisen, Chem. Phys. Lett. **213**, 514 (1993).
[46]B. I. Dunlap, J. W. D. Connolly, and J. R. Sabin, J. Chem. Phys. **71**, 3396 (1979).
[47]J. L. Whitten, J. Chem. Phys. **58**, 4496 (1973).
[48]N. O. C. Winter and C. Hättig, J. Chem. Phys. **134**, 184101 (2011).
[49]TURBOMOLE V7.5 2020, a development of University of Karlsruhe and Forschungszentrum Karlsruhe GmbH, 1989–2007, TURBOMOLE GmbH, since 2007; available from https://www.turbomole.org.
[50]C. Hättig, A. Hellweg, and A. Köhn, Phys. Chem. Chem. Phys. **8**, 1159 (2006).
[51]C. Møller and M. S. Plesset, Phys. Rev. **46**, 618 (1934).
[52]T. H. Dunning, Jr., J. Chem. Phys. **90**, 1007 (1989).
[53]J. Kauczor, P. Norman, and W. A. Saidi, J. Chem. Phys. **138**, 114107 (2013).
[54]F. Weigend, A. Köhn, and C. Hättig, J. Chem. Phys. **116**, 3175 (2001).
[55]R. D. Amos, N. C. Handy, P. J. Knowles, J. E. Rice, and A. J. Stone, J. Chem. Phys. **89**, 2186 (1985).
[56]A. Brown, C. M. Kemp, and S. F. Mason, J. Chem. Soc. A **1971**, 751.
[57]M. S. Newman, R. S. Darlak, and L. L. Tsai, J. Am. Chem. Soc. **89**, 6191 (1967).
[58]W. S. Brickell, A. Brown, C. M. Kemp, and S. F. Mason, J. Chem. Soc. A **1971**, 756.
[59]O. E. Weigang, J. A. Turner, and P. A. Trouard, J. Chem. Phys. **45**, 1126 (1966).
[60]C. Goedicke and H. Stegemeyer, Tetrahedron Lett. **11**, 937 (1970).
[61]F. Furche, R. Ahlrichs, C. Wachsmann, E. Weber, A. Sobanski, F. Vögtle, and S. Grimme, J. Am. Chem. Soc. **122**, 1717 (2000).
[62]A. Köhn, "Analytische gradienten elektronisch angeregter Zustände und Behandlung offenschaliger systeme im Rahmen der coupled-cluster-methode RI-CC2," Ph.D. thesis, Fakultät für Chemie und Biowissenshaften der Universität Karlsruhe, 2003.
[63]S. Abbate, G. Longhi, F. Lebon, E. Castiglioni, S. Superchi, L. Pisani, F. Fontana, F. Torricelli, T. Caronna, C. Villani, R. Sabia, M. Tommasini, A. Lucotti, D. Mendola, A. Mele, and D. A. Lightner, J. Phys. Chem. C **118**, 1682 (2014).
[64]V. Buss and K. Kolster, Chem. Phys. **203**, 309 (1996).
[65]Y. Nakai, T. Mori, and Y. Inoue, J. Phys. Chem. A **116**, 7372 (2012).
[66]R. H. Martin and M. J. Marchant, Tetrahedron **30**, 343 (1974).
[67]A. Kumar and W. J. Meath, Mol. Phys. **90**, 389 (1997).
[68]A. Kumar and W. J. Meath, Mol. Phys. **75**, 311 (1992).
[69]B. L. Jhanwar and W. J. Meath, Mol. Phys. **41**, 1061 (1980).
[70]A. Kumar, B. L. Jhanwar, and W. Meath, Can. J. Chem. **85**, 724 (2007).
[71]G. F. Thomas and W. J. Meath, Mol. Phys. **34**, 113 (1977).
[72]A. Kumar and A. J. Thakkar, Chem. Phys. Lett. **516**, 208 (2011).
[73]A. Ruzsinszky, J. P. Perdew, J. Tao, G. I. Csonka, and J. M. Pitarke, Phys. Rev. Lett. **109**, 233203 (2012).
[74]W. A. Saidi and P. Norman, J. Chem. Phys. **145**, 024311 (2016).